J Low Temp Phys (2009) 157: 429–475
DOI 10.1007/s10909-009-9994-8

Particles-Vortex Interactions and Flow Visualization in ^{4}He

Y.A. Sergeev · C.F. Barenghi

Received: 27 March 2009 / Accepted: 27 September 2009 / Published online: 14 October 2009

Abstract Recent experiments have demonstrated a remarkable progress in implementing and use of the Particle Image Velocimetry (PIV) and particle tracking techniques for the study of turbulence in ^{4}He. However, an interpretation of the experimental data in the superfluid phase requires understanding how the motion of tracer particles is affected by the two components, the viscous normal fluid and the inviscid superfluid. Of a particular importance is the problem of particle interactions with quantized vortex lines which may not only strongly affect the particle motion, but, under certain conditions, may even trap particles on quantized vortex cores. The article reviews recent theoretical, numerical, and experimental results in this rapidly developing area of research, putting critically together recent results, and solving apparent inconsistencies. Also discussed is a closely related technique of detection of quantized vortices by negative ion bubbles in ^{4}He.

Keywords Superfluids · Vortices and turbulence · Particle-vortex interactions · Flow visualization

PACS 67.40.Vs · 47.37.+q · 47.27.-i

1 Introduction and Plan of the Review

In this review we will be mostly concerned with the motion of small solid particles in turbulent ^{4}He. This new and rapidly developing area of research has been initiated

Y.A. Sergeev (✉)
School of Mechanical and Systems Engineering, Newcastle University, Newcastle upon Tyne, NE1 7RU, England, UK
e-mail: yuri.sergeev@ncl.ac.uk

C.F. Barenghi
School of Mathematics and Statistics, Newcastle University, Newcastle upon Tyne, NE1 7RU, England, UK

by the recent success of implementation of the Particle Image Velocimetry (PIV) and the particle tracking techniques in superfluid helium, see Donnelly et al. [1], Van Sciver and co-workers [2–6], and publications of the group involving Paoletti, Bewley, Lathrop, Sreenivasan and their co-workers [7–11]. (The only difference between these two, otherwise identical, techniques is that the results of PIV yield the local average particle velocities obtained by calculating cross-correlations of particle ensembles and, therefore, result in the fluid-like, smooth velocity field, while the particle tracking aims at investigation of individual particle trajectories.) These are perhaps the only two well developed techniques which can identify the flow patterns in turbulent superfluid helium. The PIV has been a standard technique in classical fluid dynamics for several decades (see, for example, the book by Raffel et al. [12]). In experimental studies of classical turbulence, one can be confident that the motion of sufficiently small particles will reveal the details of turbulent motion of the viscous fluid. In superfluids, the two-fluid nature of ^{4}He makes an interpretation of PIV measurements much more difficult: A solid particle interacts with both the normal fluid and the superfluid; moreover, the particle may interact strongly with quantized vortex lines in the superfluid component, and even become trapped on them.

The mechanism of trapping of solid particles is essentially the same as that of trapping the charge carriers on quantized vortices in ^{4}He, primarily because e.g. the negative ion (electron) forms around itself an almost macroscopic bubble of radius 12–20 Å from which helium atoms are excluded. The ion trapping technique was used for detection of quantized vortices since late 50s, and, although not being suitable for studying the normal fluid patterns in ^{4}He, can be considered as the technique closely related to the PIV and the particle tracking methods. We will review the development of the ion trapping technique in Sect. 7 of this article.

The aims of experimental physicists working in the area of superfluid turbulence are to understand the vortex tangle (quantum turbulence), to measure velocity fluctuations in both the normal fluid and the superfluid, and possibly to make comparisons between quantum turbulence and ordinary turbulence. Until recently the major difficulty was lack of direct flow visualization technique near absolute zero. Existing methods, such as measurements of temperature differences to detect extra dissipation, ion trapping, measurements of second sound attenuation by quantized vortices, etc. probed only the vortex line density L (total vortex length per unit volume) averaged over an experimental cell and did not reveal turbulent velocity fluctuations (although a remarkable resolution has been recently achieved in second sound measurements by Roche et al. [13] of the local tangle density).

Experimental breakthrough was made in 2002 when the PIV technique was successfully introduced in ^{4}He (see references in the first paragraph of this section). This technique, which has been standard in classical fluid dynamics for many years, is based on injecting many small particles into the liquid. Two images are produced using short laser pulses of different frequencies (corresponding e.g. to the green and red colors) focused into a narrow sheet and separated in time by a few milliseconds. Software then analyzes the images and identifies green and red dots corresponding to the same particle at the two different times. In this way the observed distance between the corresponding dots yields the component of the local velocity in the plane of the light sheet.

In classical fluids, provided the particle size is sufficiently small (in turbulence studies, "small" means smaller than the Kolmogorov length), the dominating force acting on the particle is the viscous drag force, so that a researcher can be confident that small particles trace the fluid motion (in particular, turbulent velocity fluctuations) rather well.

Because the viscosity of liquid helium is very low the Kolmogorov scale in the turbulent normal fluid can be very small, so that it is essential that the particles used in visualization experiments are as small as possible. In the cited experimental works the typical particle diameter was of the order of 1 μm.

What do tracer particles trace in superfluid helium? One may expect that, although the viscosity of ^{4}He is low, the dominating force exerted on the particle by the fluid will still be the viscous drag, so that solid particles should trace the normal fluid. However, this is not always true: due to the two-fluid nature of superfluid helium, the particles interact not only with the normal fluid, but also with the superfluid component through inertial and added mass forces; moreover, the particles interact strongly with quantized vortices in superfluid and may even be trapped on superfluid vortex lines. Therefore, if we want to interpret results of PIV and particle tracking measurements correctly, we must answer first the question asked in the beginning of this paragraph.

This article is divided in sections where theoretical and numerical models of increasing complexity are compared to each other and to experimental results. The first model, described in Sect. 2, is the one-way coupling model. In Sects. 2.1 and 2.2 we derive the governing equations of motion of particle tracers in the presence of two imposed fluids, the viscous normal fluid and the inviscid superfluid, under the assumptions that the particles do not disturb the flow, are smaller than any flow scale of interest, and do not become trapped in vortices. The one-way coupling model allows us to discuss the problem of the stability of particles' trajectories, which is relevant to the visualization of a pure superflow. The one-way coupling model is powerful enough to derive the general principles which lead to particles being trapped on vortices. In Sect. 2 we present the experimental evidence for this trapping (Sect. 2.3), and show how the mutual friction affect the motion of particles near vortex cores (Sect. 2.4). Three case studies are discussed of particle trajectories near vortices: vortex ring, thermal counterflow tangles, and vortex tangles at low temperatures (Sect. 2.5).

Section 3 introduces the more sophisticated (and computationally more expensive) two-way coupling model; in this model the back reaction of the flow on the particle is taken into account, and the dynamics of the particle-vortex interaction and the trapping can be studied in great detail, including what happens at the surface of the particle (which we assume to be spherical for simplicity). Section 3.1 contains the mathematical formulation of the two-way coupling model; Sects. 3.2 and 3.3 are devoted to the numerical calculations of typical vortex-particle interactions.

Section 4 makes use of the results of the numerical simulations described in Sect. 3 to derive a simpler analytical model which explains in a quantitative way experiments performed in Florida [2–6] in which heavy particles fell through a tangle of vortices. The two-way coupling model is also applied to particles moving in tangles generated by a thermal counterflow: these numerical results are applied to particle-tracking experiments performed in Maryland [7–11]. By considering numerical calculations at

small and high values of the vortex line density, we solve the apparent disagreement between the Florida and Maryland experiments: the discussion will reveal that the two experiments refer to two different regimes, which are both explained by the two-way coupling model. In Sect. 4 we also discuss the experimental observation of flow structures observed behind and in front a cylindrical obstacle set in the middle of a counterflow channel, and propose a simple analytical two-dimensional model which accounts, at least in principle, for the qualitative existence of these flow structures.

Section 5 describes the most recent experimental discoveries obtained using tracer particles: the observation of turbulent boundary layer flows, the visualization of individual vortex reconnections, and the measurement of velocity statistics. Section 7 reviews other techniques based on trapping ions and imaging He_2 molecules; these techniques share important principles (but not the size of the trapped object) with PIV and particle tracking techniques. Section 8 contains the final discussion.

2 One-Way Coupling Model of Particle Motion in Turbulent ^{4}He

We begin answering this question with a relatively simple, "one-way coupling" model which follows the approach standard in classical two-phase turbulence studies. We will generalize to the two-fluid model of superfluid helium the equations of motion of a solid spherical particle of radius a_p in a nonuniform flow of classical fluid. We assume that (1) the presence of particles does not modify the turbulence, (2) the flow velocities vary little over a distance of the order of particle size, and (3) particles do not interact strongly with quantized vortex lines and are certainly not trapped on these lines. These assumptions require that the particle size be much smaller than both the Kolmogorov lengthscale, b_η in the normal fluid, and the mean intervortex distance, $\ell = L^{-1/2}$ in the superfluid. Below we formulate, under these assumptions, the equations of particle motion.

2.1 Fluid-Particle Interaction

We start with the fluid-particle interaction in classical liquids. We consider a spherical solid particle of radius a_p in the nonuniform flow. Let the ambient (that is, in the absence of the particle) fluid velocity field be $\mathbf{v}(\mathbf{r}, t)$. According to the assumptions formulated above, the size of the particle is much smaller than the flow lengthscale, λ, i.e. $a_p \ll \lambda$, so that we can introduce a small parameter

$$\varepsilon = a_p \|\nabla \mathbf{v}\| / |\mathbf{v} - \mathbf{u}_p| \ll 1, \tag{1}$$

where $\mathbf{u}_p$ is the particle velocity.

2.1.1 Fluid-Particle Interaction in the Inviscid Nonuniform Flow

As shown by Auton et al. [14], the total force acting on the particle in the nonuniform, inviscid flow can, under assumption (1), be represented in the form

$$\mathbf{F} = \mathbf{F}^{(\mathrm{i})} + \mathbf{F}^{(\mathrm{a})} + \mathbf{F}^{(\omega)}, \tag{2}$$

where

$$\mathbf{F}^{(\mathrm{i})} = \rho\vartheta \frac{D\mathbf{v}}{Dt} \quad \text{and} \quad \mathbf{F}^{(\mathrm{a})} = C\rho\vartheta \left(\frac{D\mathbf{v}}{Dt} - \frac{d\mathbf{u}_p}{dt} \right) \tag{3}$$

are the inertial and the added mass force, respectively, $\vartheta = \frac{4}{3}\pi a_p^3$ is the particle volume,

$$\frac{D}{Dt} = \frac{\partial}{\partial t} + (\mathbf{v} \cdot \nabla), \tag{4}$$

and C is the added mass coefficient (for spherical particle $C = \frac{1}{2}$);

$$\mathbf{F}^{(\omega)} = \frac{1}{2}\rho\vartheta(\mathbf{v} - \mathbf{u}_p) \times \boldsymbol{\omega}, \tag{5}$$

where $\boldsymbol{\omega} = \nabla \times \mathbf{v}$ is the vorticity, represents the lift force arising due to stretching of vortex lines in the vicinity of the sphere's surface.

2.1.2 Fluid-Particle Interaction in the Nonuniform Viscous Flow

We will consider the motion of a solid particle in the viscous fluid assuming that the particle Reynolds number is small:

$$\mathrm{Re}_p = a_p|\mathbf{v} - \mathbf{u}_p|/\nu \ll 1, \tag{6}$$

where ν is the kinematic viscosity. Note that small particle Reynolds numbers are typical of PIV and particle tracking experiments, both in classical fluids and in superfluid helium. We will consider the particle motion under the assumptions formulated above (in particular that the parameter ε introduced by formula (1) is small).

Detailed analysis of the forces acting on the particle in the nonuniform viscous flow can be found in works by Maxey and Riley [15], Mei [16], and Kim, Elghobashi, and Sirignano [17]. The total force acting on the particle can be represented as a sum of several contributions, i.e. the gravity, viscous drag, the inertial and added mass force, Faxén correction arising due to the local non-uniformity of the ambient flow, the Saffman lift force arising due to the local shear, and the Magnus lift force arising due to rotation of the particle.

The main contribution, dominating in most particulate flows, is the viscous Stokes drag force:

$$\mathbf{F}^{(\mathrm{d})} = 6\pi a_p \rho\nu(\mathbf{v} - \mathbf{u}_p). \tag{7}$$

Surprisingly, in the viscous flow the inertial and added mass forces, $\mathbf{F}^{(\mathrm{i})}$ and $\mathbf{F}^{(\mathrm{a})}$ are determined by the same formulae (2)–(3) as for the inviscid flow, with the same added mass coefficient, $C = \frac{1}{2}$ for the spherical particle.

2.1.3 Fluid-Particle Interaction in ^{4}He

To determine the force acting on the particle in ^{4}He, we simply add together all the forces exerted by the normal fluid and the superfluid. Since the superflow is potential,

$\mathbf{F}_s^{(\omega)}$ is identically zero, provided the particle does not become trapped on quantized vortex lines. As shown by Poole et al. [18], for the flow properties and physical parameters typical of the normal component of ^{4}He, the Faxén correction, the history and lift forces can be neglected provided the particle Reynolds number and the parameter ϵ are small and the particle size is significantly smaller than the Kolmogorov length. Therefore, the total force acting on the particle can be approximated as

$$\mathbf{F} = \mathbf{F}^{(\mathrm{g})} + \mathbf{F}_n^{(\mathrm{d})} + \mathbf{F}_n^{(\mathrm{i})} + \mathbf{F}_n^{(\mathrm{a})} + \mathbf{F}_s^{(\mathrm{i})} + \mathbf{F}_s^{(\mathrm{a})}, \tag{8}$$

where the subscripts n and s refer to the normal fluid and the superfluid, respectively. Here $\mathbf{F}^{(\mathrm{g})}$ is the combination of gravity and buoyancy, and $\mathbf{F}_n^{(\mathrm{d})}$ is the viscous drag force exerted by the normal fluid:

$$\mathbf{F}^{(\mathrm{g})} = \vartheta(\rho_p - \rho)\mathbf{g}, \qquad \mathbf{F}_n^{(\mathrm{d})} = 6\pi a_p \mu_n (\mathbf{v}_n - \mathbf{u}_p), \tag{9}$$

where μ_n is the viscosity of ^{4}He. Substantial derivatives required for determining the inertial and added mass forces in the normal and superfluid components are now defined by formula (4) with $\mathbf{v}$ replaced by $\mathbf{v}_n$ and $\mathbf{v}_s$, respectively.

2.2 Lagrangian Equations of Particle Motion

We arrive at the following equation of particle motion [18]:

$$\begin{aligned}\rho_p \vartheta \frac{d\mathbf{u}_p}{dt} &= 6\pi a_p \mu_n (\mathbf{v}_n - \mathbf{u}_p) + \vartheta(\rho_p - \rho)\mathbf{g} \\ &\quad + \rho_n \vartheta \frac{D\mathbf{v}_n}{Dt} + C\rho_n \vartheta \left(\frac{D\mathbf{v}_n}{Dt} - \frac{d\mathbf{u}_p}{dt} \right) \\ &\quad + \rho_s \vartheta \frac{D\mathbf{v}_s}{Dt} + C\rho_s \vartheta \left(\frac{D\mathbf{v}_s}{Dt} - \frac{d\mathbf{u}_p}{dt} \right).\end{aligned} \tag{10}$$

This equation must be considered together with the kinematic equation

$$d\mathbf{r}/dt = \mathbf{u}_p, \tag{11}$$

where $\mathbf{r} = \mathbf{r}(t) = (x(t), y(t), z(t))$ $(\equiv \mathbf{r}_p(t))$ should be regarded as a Lagrangian trajectory of the solid particle. Equations (10) and (11) constitute the closed system for the unknown particle position and velocity, $\mathbf{r}(t)$ and $\mathbf{u}_p(t)$, respectively.

Often (although not always) in the PIV and particle tracking experiments neutrally buoyant particles (with $\rho_p = \rho$) are used in order to eliminate unwanted effects of gravity on the particle motion. For neutrally buoyant particles, (10) can be written in a more concise form

$$\frac{d\mathbf{u}_p}{dt} = \frac{1}{\tau}(\mathbf{v}_n - \mathbf{u}_p) + \frac{3}{2\rho_o}\left(\rho_n \frac{D\mathbf{v}_n}{Dt} + \rho_s \frac{D\mathbf{v}_s}{Dt} \right), \tag{12}$$

where

$$\rho_o = \rho_p + \rho/2 = 3\rho/2 \quad \text{and} \quad \tau = 2a_p^2 \rho_o/(9\mu_n). \tag{13}$$

The parameter τ, which shows how quickly the particle adjusts its motion to the viscous flow, plays an important rôle in the study of particle motion in fluids, and is commonly known as either the particle response time, or viscous relaxation time.

Analyzing (11) and (12), Poole et al. [18] showed that, provided $\tau/\tau_f \ll 1$, where τ_f is the timescale of the fluid motion (e.g. the Kolmogorov time), the neutrally buoyant particle tracks the motion of the normal fluid. If $\tau/\tau_f \gg 1$, the particle moves with a velocity corresponding to the total current density, $\mathbf{j} = \rho_n \mathbf{v}_n + \rho_s \mathbf{v}_s$.

However, two important issues may invalidate these conclusions: (1) instability of particle trajectories, and (2) trapping of particles on superfluid vortex lines. The analysis of particle trapping will require more elaborate, self-consistent, two-way coupling model which would account for deformation of the vortex filament by the approaching particle, including possible reconnection of the vortex with the particle surface (see below Sect. 3).

2.2.1 Instability of Particle Trajectories

Instability of Lagrangian trajectories of the neutrally buoyant particle in the classical viscous fluid was discovered and studied relatively recently by Babiano et al. [19]. To illustrate such an instability in turbulent superfluid at finite temperature such that both the normal fluid and the superfluid component are present, we consider the simplest case assuming that $\mathbf{v}_n \approx \mathbf{v}_s =: \mathbf{v}$ down to the length scales comparable to the vortex line spacing. The Lagrangian equations of particle motion, which become

$$\frac{d\mathbf{u}_p}{dt} = \frac{\mathbf{v} - \mathbf{u}_p}{\tau} + \frac{D\mathbf{v}}{Dt}, \qquad \frac{d\mathbf{r}_p}{dt} = \mathbf{u}_p, \tag{14}$$

have, provided $\mathbf{u}_p(0) = \mathbf{v}(0)$ and $\mathbf{r}_p(0) = \mathbf{r}_f(0)$, a formal solution $\mathbf{u}_p(t) = \mathbf{v}(\mathbf{r}_f, t)$, $\mathbf{r}_p(t) = \mathbf{r}_f(t)$, where $\mathbf{r}_f(t)$ is a trajectory of the fluid point. Therefore, it would seem natural to conclude that neutrally buoyant particles follow the fluid exactly.

However, let us consider now the particle motion in the so-called ABC (Arnold-Beltrami-Childress) flow, frequently used as the simplest model of turbulence, whose velocity field is

$$v_x = A\sin(2\pi z) + C\cos(2\pi y), \qquad v_y = B\sin(2\pi x) + A\cos(2\pi z),$$
$$v_z = C\sin(2\pi y) + B\cos(2\pi x). \tag{15}$$

The time sequence [18] illustrating the position of large number of neutrally buoyant tracer particles in the ABC flow, starting from their uniform distribution, is shown in Fig. 1. It can be seen that particles do not follow the fluid, but instead, due to instabilities of their trajectories, travel from the regions of high vorticity to the regions of high rate of strain. (In classical multiphase fluid dynamics similar phenomenon for particles heavier than the fluid has been studied in detail. However, the mechanism of segregation of heavy particles is quite different from that of neutrally buoyant particles.) Note, though, that this instability develops rather slowly: the last frame of Fig. 1, recovering the lines of minimum vorticity and maximum rate of strain, corresponds to 3 times of turnover of the ABC flow.

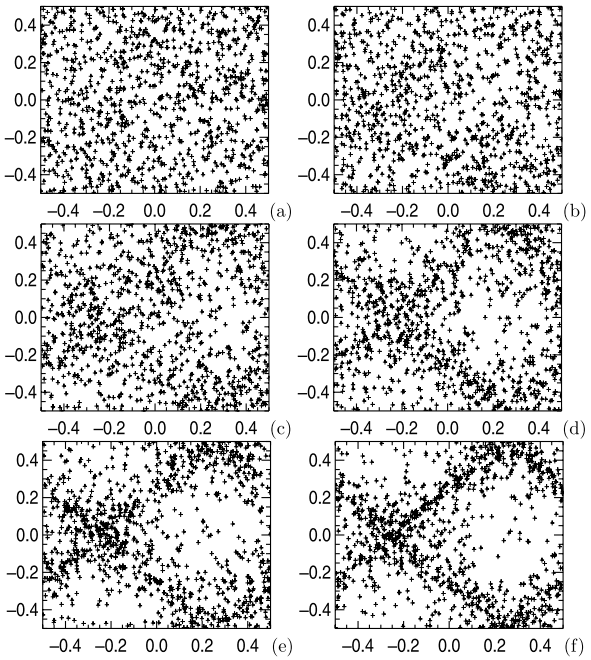

Fig. 1 Positions of tracer particles at different times [18]. From Poole, Barenghi, Sergeev, and Vinen, *Phys. Rev. B* **71**, 064514 (2005). Reprinted by permission, ©2005 American Physical Society

Instability of particle trajectories is more pronounced in the case $T \to 0$ when the normal fluid is absent. The equations of motion of neutrally buoyant particle become

$$\frac{d\mathbf{u}_p}{dt} = \frac{\partial \mathbf{v}_s}{\partial t} + (\mathbf{v}_s \cdot \nabla)\mathbf{v}_s = -\nabla p, \qquad \frac{d\mathbf{r}_p}{dt} = \mathbf{u}_p, \tag{16}$$

and have a formal solution $\mathbf{u}_p(t) = \mathbf{v}_s(\mathbf{r}_s(t), t)$, $\mathbf{r}_p(t) = \mathbf{r}_s(t)$, where $d\mathbf{r}_p/dt = \mathbf{v}_s(\mathbf{r}_s, t)$, so that, in the case of very low temperature when the normal fluid is absent, it can be expected that neutrally buoyant particles trace the superfluid. However, this is not the case either. Consider the simplest case of the neutrally buoyant particle moving around a single, stationary, straight vortex line. In cylindrical polar coordinates (r_p, θ_p) the equations of particle motion are:

$$\ddot{r}_p - r_p\omega_p^2 = -\kappa^2/(2\pi^2 r_p^3), \qquad 2\omega\dot{r}_p + r_p\dot{\omega}_p = 0, \tag{17}$$

where $\omega_p = \dot{\theta}_p$. If at the initial moment the particle velocity does not coincide exactly with the fluid velocity, the particle will spiral either outwards, or inwards. We arrive at the conclusion which remains valid in the general case of particle motion at temperature $T \to 0$ (Sergeev et al. [20]): unless the initial velocity of neutrally buoyant particle matches exactly the velocity of the fluid point, the trajectory of the solid particle deviates significantly from the trajectory of the fluid point. Such an instability is amplified by any macroscopic mismatch between the velocity of the superfluid and the velocity of the particle at the beginning of the experiment. This is further illustrated by Fig. 2 showing the trajectories of solid and fluid particles around three vortices.

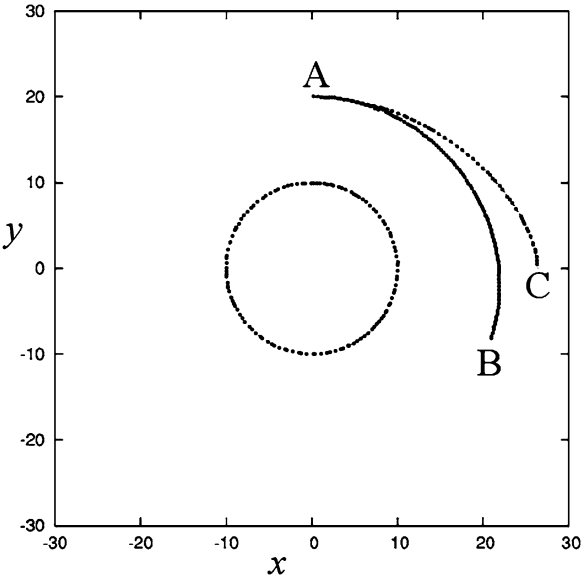

Fig. 2 Trajectories [20] of neutrally buoyant solid particle (dashed line A to C) and superfluid particle (solid line A to B) around three vortices moving along the closed orbit shown. From Sergeev, Barenghi, Kivotides, and Vinen, *Phys. Rev. B* **73**, 052502 (2006). Reprinted by permission, ©2006 American Physical Society

2.3 Trapping of Particles on Quantized Vortices: Mechanism and Experimental Evidence

2.3.1 Mechanism

Why can the superfluid vortex trap the particle? To answer this question, we have to take into account a possibility of reconnection of the quantized vortex to the surface of moving particle (a more detailed analysis of the mechanism of this process will be given below in Sect. 3).

Below three different versions, or, rather, three different ways of explaining the reason for particle trapping are suggested.

1°. Imagine that the quantized vortex reconnects symmetrically to the surface of spherical particle, as shown in the right part of Fig. 3. The kinetic energy of the flow field created by the straight quantized vortex can be easily calculated, and in the symmetric configuration is reduced by

$$\Delta E = \frac{\rho_s \kappa^2 a_p}{2\pi} \ln \frac{2a_p}{\xi}, \tag{18}$$

where $\xi \approx 10^{-8}$ cm is the vortex core radius. Note that assuming $a_p \gg \xi$ this result follows from the substitution energy calculated by Parks and Donnelly [21] for the ion bubble trapped by the quantized vortex line, see below Sect. 7 and formula (38) therein. Formula (18) determines the kinetic energy which the particle would require to break free from the symmetric vortex configuration shown in Fig. 3 (right).

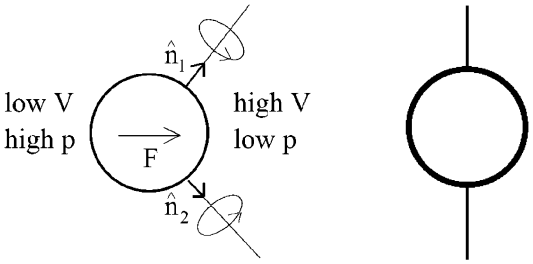

Fig. 3 Asymmetric reconnection of the vortex to the particle surface creates a force restoring the symmetric particle-vortex configuration [22]. From Sergeev, Barenghi, and Kivotides, *Phys. Rev. B* **74**, 184506 (2006). Reprinted by permission, ©2006 American Physical Society

2°. The flow field of the vortex creates a pressure gradient

$$\nabla p = -\rho_s(\mathbf{v}_s \cdot \nabla)\mathbf{v}_s = \frac{\rho_s \kappa^2}{8\pi^2}\nabla\left(\frac{1}{r^2}\right) \tag{19}$$

attracting the particle to the vortex.

3°. If the particle-vortex configuration is symmetric, as in the right part of Fig. 3, then, obviously, the force acting on the particle is zero. Now imagine that this symmetry is perturbed as shown in the left part of this figure. The superfluid component is inviscid, so that the following arguments apply based on Bernoulli's integral: the fluid velocity on the right side of the particle surface, where the two vortex strands are closer, is greater than that on the left side, and, therefore, the pressure is bigger on the left side of the sphere. This provides a net force restoring the symmetric particle-vortex configuration.

2.3.2 Evidence of Particle Trapping

Experimental evidence comes from the publication of Bewley, Lathrop and Sreenivasan [7] (see also more recent papers [9–11]). Figure 4, published in the cited paper [7], shows that the researchers, using the PIV technique, actually "painted" quantized vortices by tracer particles.

Another evidence comes not from experiments, but from the quantum calculation based on the Gross-Pitaevskii equation. Berloff and Roberts [23] studied an interaction between the negative ion and the quantized vortex. In superfluid helium, the negative ion forms around itself a bubble of diameter approximately 16×10^{-8} cm (an order of magnitude higher than the size of the vortex core, $\xi \approx 10^{-8}$ cm) and, therefore, can be treated, for our purpose, as a particle (albeit very small). Results of Berloff and Roberts' calculation are illustrated in Fig. 5: the ion bubble approaches the vortex, which deforms (b) and (c) and then reconnects to the particle surface (d); the reconnection excites Kelvin waves (f), (g), and (h) which carry away the energy, and, eventually, the bubble-vortex configuration relaxes and the ion becomes trapped on the vortex core (i).

2.4 Mutual Friction and Trapping

At this point, the question can be asked whether it is worth or not further exploiting the one-way coupling model which neglects any influence of the particle on the vortex

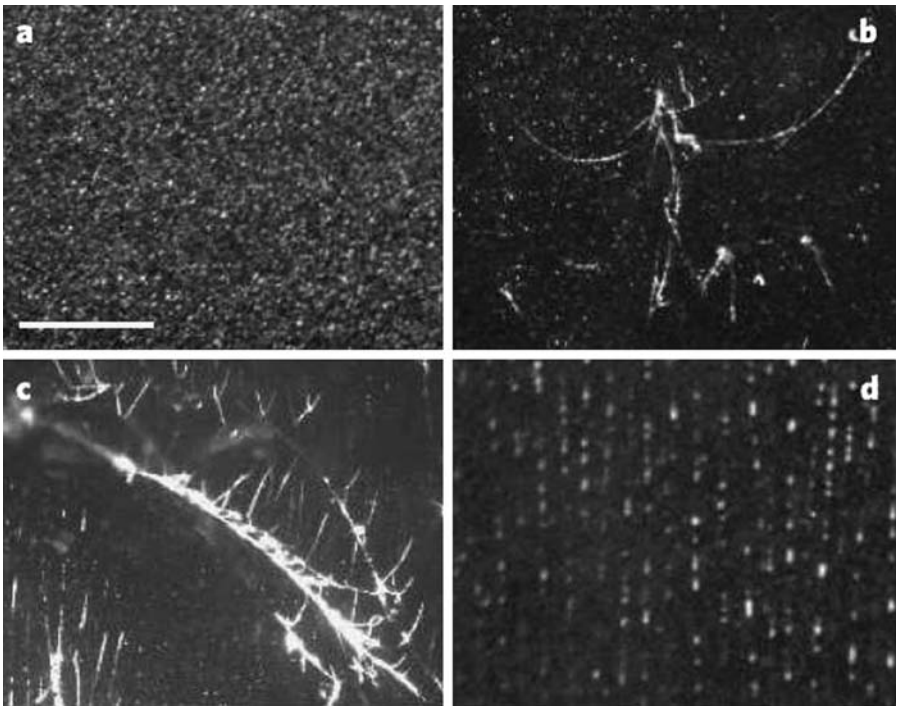

Fig. 4 PIV visualization [7] by Bewley, Lathrop, and Sreenivasan (*Nature* **441**, 588 (2006)) of quantized vortex cores: (**a**) above λ transition; (**b**) and (**c**) branching filaments tenth of mK below λ transition; (**d**) regrouping along vertical lines in steady rotating apparatus. Reprinted by permission, ©2006 Macmillan Publishers Ltd.

evolution. The answer is "yes": there are cases where trapping events are not very frequent, so that a useful information about the behavior of tracer particles can be obtained by ignoring their trapping on vortex cores. We will also show that the mutual friction between quantized vortices and the normal fluid can prevent trapping.

In the vicinity of the vortex core, the mutual friction induces, in the normal fluid, the vortex dipole whose typical lengthscale is expected to be about 100 μm. The results of numerical calculation by Idowu et al. [24] of the dipole-like normal fluid disturbance are shown in Fig. 6. This normal flow disturbance can deflect the tracer particle which otherwise would have collided with, and possibly trapped by the vortex. Typical trajectory, calculated by Sergeev et al. [25], of the particle moving from right to left and interacting with the superfluid vortex and normal fluid disturbance is shown in Fig. 7 by the solid line. For comparison, the trajectory calculated without taking into account the normal fluid disturbance is shown by the dashed line. This trajectory leads to the collision with the vortex core located at the origin.

Normal fluid vortical structures induced by the mutual friction were predicted by Hall and Vinen [26] and Kivotides, Barenghi, and Samuels [27], but so far, because of low resolution of experimental techniques, there was no direct experimental proof of existence of the normal fluid disturbances. Owing to the much higher resolution, the PIV and particle tracking techniques can provide such an evidence. Perhaps the

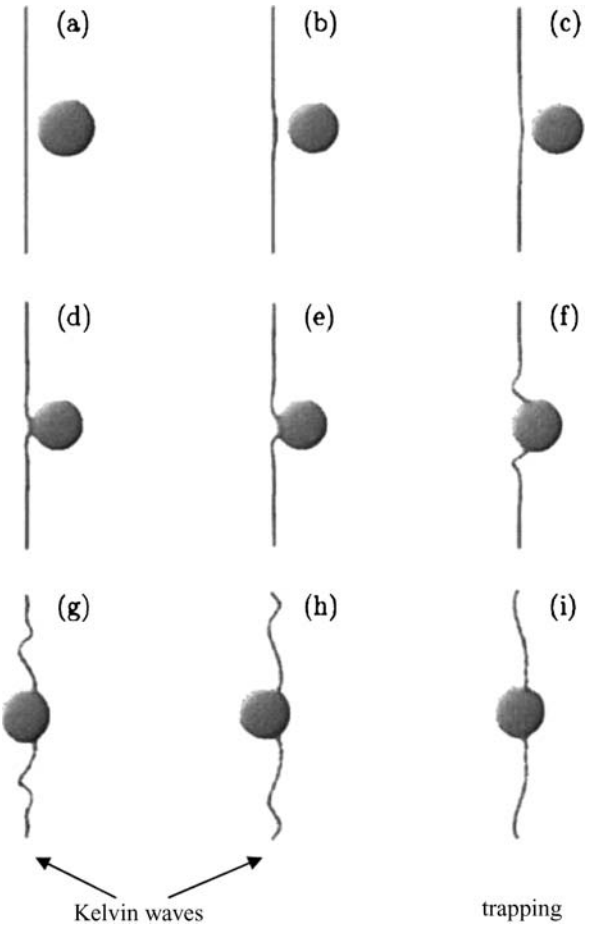

Fig. 5 Trapping of the ion bubble by the quantized vortex: microscopic calculation [23] by Berloff and Roberts (*Phys. Rev. B* **63**, 024510 (2000)) based on the Gross-Pitaevskii equation. Reprinted by permission, ©2000 American Physical Society

first experimental confirmation of existence of normal flow structures induced by the mutual friction has already been found. Figure 8 shows a typical particle trajectory observed by Bewley, Lathrop, Sreenivasan, and Paoletti [28], by means of the particle tracking technique, in the thermal counterflow. The particle trajectory has characteristic 'kinks' resembling the 'deflected' trajectory shown by the solid line in Fig. 7.

In the remaining part of this section we will analyze, neglecting trapping, three examples of particle motion in ^{4}He.

2.5 Case Studies

2.5.1 Vortex Ring Propagating Against a Particulate Sheet

This study [29] led to a proposal of a simple experiment (not performed yet) which could, in principle, justify the use of PIV technique for measuring instantaneous normal fluid velocity patterns. We consider a single vortex ring propagating normally to a plane sheet of neutrally buoyant particles, see Fig. 9 (left).

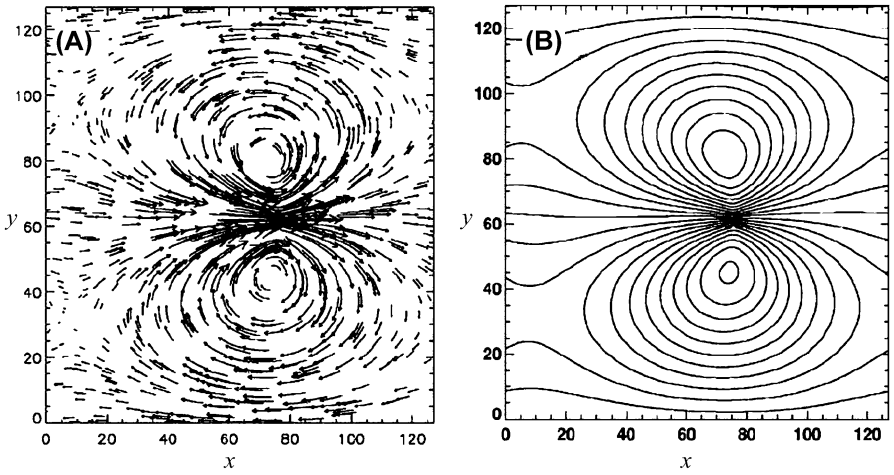

Fig. 6 Velocity field of the normal fluid due to the mutual friction forcing of a single superfluid vortex [24]. (**A**) Velocity arrow plot; (**B**) Streamlines. From Idowu, Willis, Barenghi, and Samuels, *Phys. Rev. B* **62**, 3409 (2000). By permission, ©2000 American Physical Society

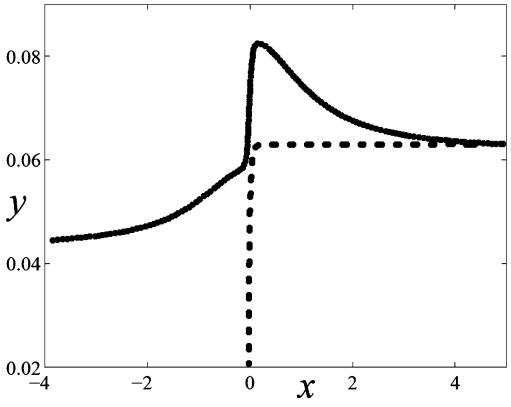

Fig. 7 Particle trajectories [25] in the presence (*solid lines*) and absence (*dashed line*) of the normal fluid disturbances. From Sergeev, Wang, Meneguz, and Barenghi, *J. Low Temp. Phys.* **146**, 417 (2007). Reprinted by permission, ©2007 Springer

In the considered model, the mutual friction between the normal fluid and the superfluid vortex is taken into account leading to emergence of the normal fluid disturbances described earlier. The motion of the superfluid vortex whose core is defined parametrically by $\mathbf{X}(s,t)$ is governed by the following equation derived by Idowu et al. [30]:

$$\partial\mathbf{X}/\partial t = \mathbf{v}_\ell = h\mathbf{V}^{\mathrm{s}} + h_*\mathbf{X}' \times (\mathbf{v}_n - \mathbf{V}^{\mathrm{s}}) - h_{**}\mathbf{X}' \times (\mathbf{X}' \times \mathbf{v}_n), \tag{20}$$

where $\mathbf{X}' = \partial\mathbf{X}/\partial s$, $h(T)$, $h_*(T)$ and $h_{**}(T)$ are the known mutual friction coefficients, and the vortex-induced superfluid velocity $\mathbf{V}^{\mathrm{s}}$ is given by the Biot-Savart integral

$$\mathbf{V}^{\mathrm{s}}(\mathbf{x}) = -\frac{\kappa}{4\pi}\int ds \frac{\mathbf{X}' \times (\mathbf{X} - \mathbf{x})}{|\mathbf{X} - \mathbf{x}|^3}. \tag{21}$$

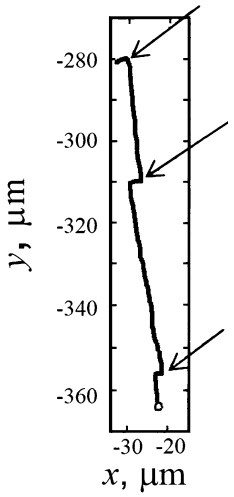

Fig. 8 Observation by Bewley, Lathrop, Sreenivasan, and Paoletti [28] of particle trajectories possibly indicating an influence of normal fluid disturbances induced by the mutual friction

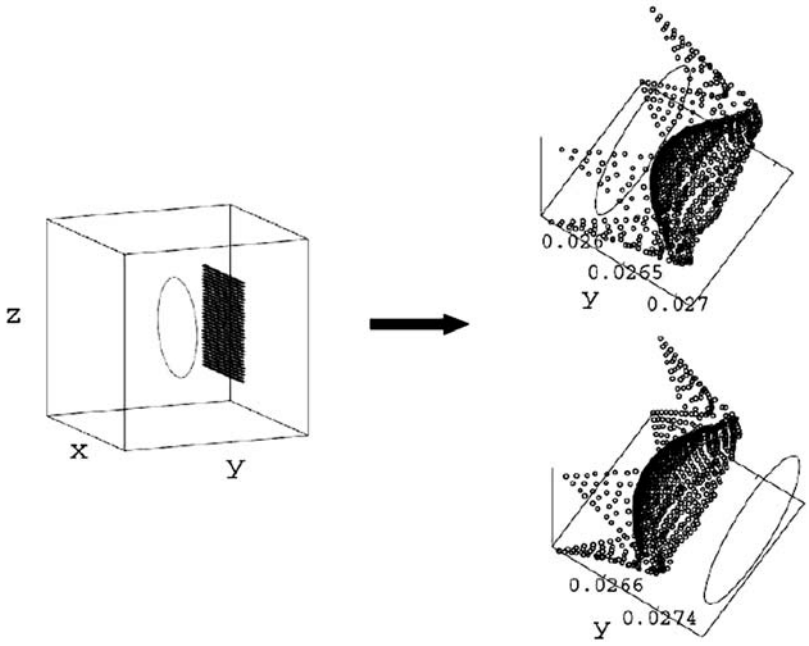

Fig. 9 Vortex ring and solid particles' configurations before and after the ring has passed through the particulate sheet [29]. Adapted from Kivotides, Barenghi, and Sergeev, *Phys. Rev. Lett.* **95**, 215302 (2005). By permission, ©2005 American Physical Society

The motion of incompressible ($\nabla \cdot \mathbf{v}_n = 0$) normal fluid is governed by the equation

$$\frac{\partial \mathbf{v}_n}{\partial t} + (\mathbf{v}_n \cdot \nabla)\mathbf{v}_n = -\frac{1}{\rho}\nabla p + \nu \nabla^2 \mathbf{v}_n + \frac{1}{\rho}\mathbf{F}, \tag{22}$$

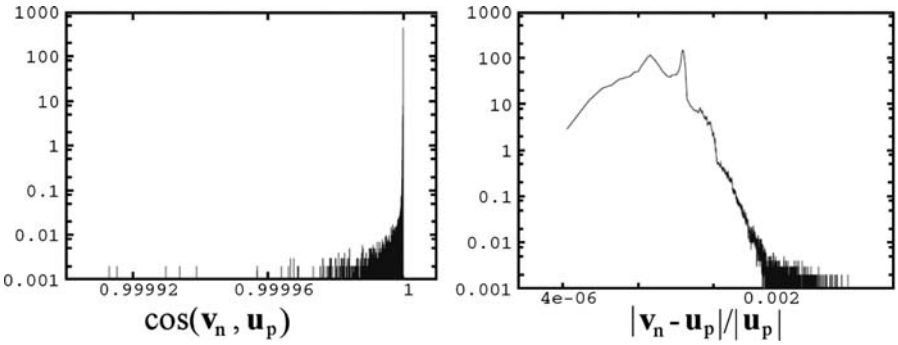

Fig. 10 Histograms [29] of the cosine of the angle between $\mathbf{v}_n$ and $\mathbf{u}_p$ (*left*) and of the magnitude of relative velocity, $|\mathbf{v}_n - \mathbf{u}_p|$ (*right*). The vertical axes are divided by 1000. From Kivotides, Barenghi, and Sergeev, *Phys. Rev. Lett.* **95**, 215302 (2005). Reprinted by permission, ©2005 American Physical Society

where $\mathbf{F}$ is the mutual friction force per unit volume. This force is determined as the sum of the drag force and the Iordanskii force, $\mathbf{f}$, per unit length:

$$\mathbf{f} = \rho_s \kappa [d_{**}\mathbf{X}' \times (\mathbf{X}' \times (\mathbf{v}_n - \mathbf{V}^s)) - d_*\mathbf{X}' \times (\mathbf{v}_n - \mathbf{V}^s)]. \tag{23}$$

Here the new mutual friction coefficients, $d_*(T)$ and $d_{**}(T)$ are known and can be expressed explicitly through $h(T)$, $h_*(T)$ and $h_{**}(T)$.

Trajectories of neutrally buoyant particles were found by numerical integration of (11) and (12). Configurations of solid particles before and after the ring has passed the particulate sheet are shown in Fig. 9 (right). Figure 10 shows the histograms of the angle and of the relative difference between $\mathbf{v}_n$ and $\mathbf{u}_p$; it can be seen that $\mathbf{v}_n$ and $\mathbf{u}_p$, to a very good degree of accuracy, are identical both in magnitude and direction. Moreover, the calculation showed that trapping events are relatively rare—only 42 out of 900 particles approached the ring to a distance smaller than three particle diameters. This enables us to conclude that, in the proposed experiment, the measurement of particle velocities can provide direct information about instantaneous normal flow patterns.

Later, based on the self-consistent, two-way coupling model, Kivotides and Wilkin [31] performed more elaborate study of interactions between solid particles and vortex rings, see below Sect. 3.4.

2.5.2 Particle Motion in Thermal Counterflow

In this example [32] we will be concerned with the T-I state of ^{4}He turbulence such that the vortex tangle in the superfluid component is present but the normal flow is laminar. For simplicity, the normal flow is assumed uniform, $\mathbf{v}_n = \mathbf{const}$. The superfluid velocity can be represented as $\mathbf{v}_s = \mathbf{v}_s^C + \mathbf{V}^s$, where the mean (counterflow) superfluid velocity, $\mathbf{v}_s^C$ is linked with the normal fluid velocity by the relation $\rho \mathbf{v}_s^C + \rho_n \mathbf{v}_n = \mathbf{0}$, and $\mathbf{V}^s$ is the fluctuating superfluid velocity induced by the vortex tangle. The dynamic vortex tangle is modeled, in the periodic box, taking into account the mutual friction between the normal fluid and quantized vortices, as well as

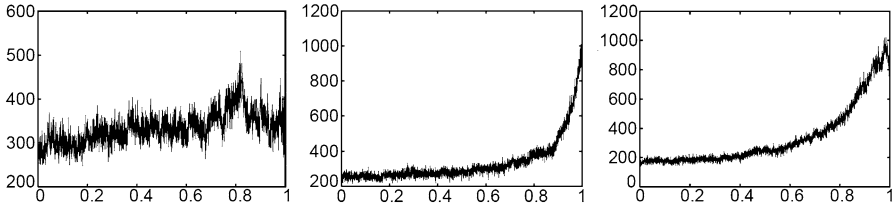

Fig. 11 Histograms [32] of $|\cos(\mathbf{V}^s, \mathbf{u}_p)|$. From Kivotides, Barenghi, and Sergeev, *Europhys. Lett.* **73**, 733 (2006). Reprinted by permission, ©2006 EDP Sciences

the Biot-Savart interaction between vortex filaments. An influence of superfluid vortices on the motion of normal fluid is neglected. Based on (11) and (12), the motion of neutrally buoyant tracer particles of diameter $d_p = 6.25 \times 10^{-3}$ cm was calculated after the vortex tangle has reached the statistically steady state. Calculations, performed at temperature $T = 1.3$ K for $|\mathbf{v}_n| = 1.1417$ and 0.6058 cm/s (corresponding values of the counterflow heat flux are $q = 1.07 \times 10^{-3}$ and 4.57×10^{-4} J/(cm$^2 \cdot$ s)), and at temperature $T = 2.171$ K for $|\mathbf{v}_n| = 0.01183$ cm/s ($q = 0.125$ J/(cm$^2 \cdot$ s)), showed that the particle velocity is very narrowly peaked around the constant normal velocity.

Three histograms of Fig. 11, corresponding to the three cases considered above, show the absence of alignment (left) between particle velocities and the superfluid velocity, $\mathbf{V}^s$ induced by the vortex tangle, and illustrate anisotropy in $\mathbf{V}^s$ (center and right).

The above two examples enable us to expect that, in the range of parameters typical of PIV measurements, neutrally buoyant particles should trace the normal fluid well, and, provided strong interactions of particles with quantized vortices can be neglected, particle velocity fluctuations induced by interactions between particles and quantized vortices should be relatively small. However, these conclusion can be invalidated by trapping of solid particles on quantized vortex cores. This phenomenon will be addressed below in Sect. 3.

2.5.3 Particle Motion in a Vortex Tangle at Very Low Temperature

Below the results discussed in Sect. 3.3 will suggest that at temperature $T < 0.5$ K, when the normal fluid is practically absent and the damping force on the particle can be neglected, trapping of neutrally buoyant solid particles on quantized vortices can, most likely, be ignored and the motion of solid particle can be modeled by a simpler, one-way coupling model. However, at these temperatures the presence and motion of the particles still affect the vortex filaments, so that a certain modification should be necessary of the one-way coupling model. In order to understand some features of the particle motion in the vortex tangle at such a low temperature, we start with a simple, two-dimensional model of the tangle [33]. In such a model the vortex lines become vortex points, and the Biot-Savart law reduces to a simple statement that each vortex point moves as a fluid point in a flow field created by all other vortices. (Such a two-dimensional system of vortex points is known as the Onsager's point vortex gas [34].)

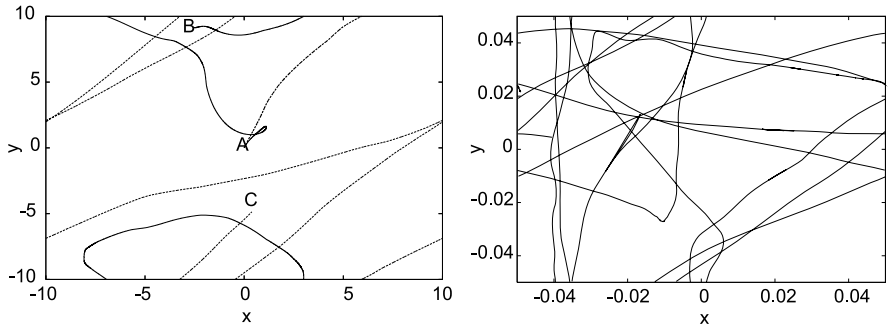

Fig. 12 *Left*: trajectories of a solid particle (*dashed line*) and of a fluid point (*solid line*) in a system of 20 vortex points. *Right*: projection of the particle trajectory in the three-dimensional vortex tangle [33]. From Kivotides, Sergeev, and Barenghi, *Phys. Fluids* **20**, 055105 (2008). Reprinted by permission, ©2008 American Institute of Physics

We consider, in the periodic box, the motion of neutrally buoyant particles in the system of vortex points of random polarity. We neglect trapping of particles on quantized vortices as well as any influence of particles on the motion of vortex points.

In this approximation the particle motion is governed by (16), and the following problem can be immediately identified: in the case where the position of the particle coincides with that of the vortex point, the pressure gradient force, $-\nabla p$ becomes unphysically singular. Based on the mechanism, described below in Sect. 3 of the particle-vortex collision at very low temperature (in the absence of damping force), we will resolve this manifest difficulty by modifying the model (16) as follows.

The cause of the problem is that in the real, three-dimensional tangle at temperature $T < 0.5$ K, even when the particle breaks through the vortex, it nevertheless reconnects with the vortex filament when the distance between the particle and the vortex core becomes of the order of particle radius. Since the vortex line attached to the particle is necessarily orthogonal to the particle surface, the reconnection results in a dramatic decrease of the force exerted on the particle; this force is zero when the particle-vortex configuration is symmetric. Then, the one-way coupling model can be modified by assuming that there exists a force-free region for $r_p < a_c$, where $a_c \sim O(a_p)$ is a cut-off distance.

In the two-dimensional calculation we set $a_c = a_p$. Trajectories of an inertial particle and a fluid point are illustrated in Fig. 12 (left) for a system of 20 vortex points set, initially, at random locations. The solid particle starts its motion at the point A where it has the velocity equal that of the fluid particle, but very quickly the trajectory of the solid particle looses any resemblance to the trajectory of the fluid point; moreover, the trajectory of the solid particle soon acquires the ballistic character. The reason for such a behavior of the solid particle is the instability of its trajectory as discussed in Sect. 2.2.1.

The evolution of particle velocity with time reveals another, rather unexpected feature: although $|\mathbf{u}_p(0)| = |\mathbf{v}_s(0)|$, the magnitude of particle velocity quickly increases above that of the fluid point, $|\mathbf{v}_s(t)|$ and eventually saturates remaining larger than the average value of $|\mathbf{v}_s|$ at all times. The average saturated particle velocity satisfies

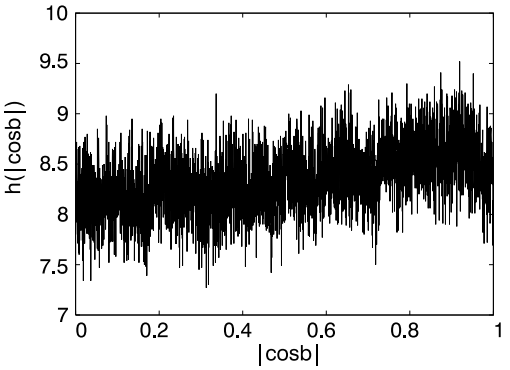

Fig. 13 Histogram [33] of the angle b between $\mathbf{u}_p$ and $\mathbf{v}_s$ (vertical axis is divided by 100). From Kivotides, Sergeev, and Barenghi, *Phys. Fluids* **20**, 055105 (2008). Reprinted by permission, ©2008 American Institute of Physics

the scaling

$$\langle u_p \rangle \sim \langle v_s \rangle \sqrt{\ell / a_c}, \tag{24}$$

where ℓ is the intervortex spacing, and $\langle v_s \rangle = \kappa/(2\pi\ell)$ the average superfluid velocity.

Using Schwarz's method [35, 36], the three-dimensional calculation of the particle motion in the vortex tangle was performed in the periodic box. The numerical technique was described by Samuels et al. [37, 38]. The motion, governed by (16), of micron-size, neutrally buoyant particle was studied in the statistically steady state of the vortex tangle. In the three-dimensional case there is no need to explicitly introduce a force-free region for distances $r_p < a_c$ from the vortex core: in Biot-Savart calculations, the normalization of the velocity when the solid particle approaches too close to a vortex is achieved by the numerical cut-off of the pressure gradient force acting on the particle, and a force-free region is automatically provided by the discretization along the vortex filament.

Figure 12 (right) shows the typical trajectory, projected on the (x, y)-plane, of the solid particle. This trajectory has the same features as the two-dimensional trajectory. Likewise, the phenomenon is observed as well of particle velocity saturation at values of $\langle u_p \rangle$ much higher than $\langle v_s \rangle$. In the three-dimensional case the calculated average particle velocity also agrees with scaling (24).

These results, together with the histogram, illustrated by Fig. 13, of the angle b between $\mathbf{u}_p$ and the superfluid velocity $\mathbf{v}_s$ suggest that from the point of view of flow visualization, in the low temperature limit (at $T < 0.5$ K) the trajectories of solid particles do not reveal flow patterns of the superfluid.

3 Self-consistent, Two-Way Coupling Model of Particle-Vortex Interactions. Particle Trapping on Quantized Vortices

The problem of particle trapping on quantized vortices constitutes a part of a wider problem of reconnections of quantized vortices with the surface of the particle moving in the fluid velocity field. This problem cannot be analyzed based on the one-way coupling model introduced in Sect. 2. Instead, a more elaborate, two-way coupling

model was developed by Kivotides, Barenghi, and Sergeev [33, 39–43] based on dynamically self-consistent calculations which take into account an influence of the flow field around the sphere on the evolution of the superfluid vortex.

3.1 Mathematical Formulation

The evolution of the vortex filament represented as a space curve $\mathbf{X}(s,t)$, where s is the arclength, is governed by the equation

$$\partial\mathbf{X}/\partial t = \mathbf{V}^{\mathrm{s}} + \mathbf{V}^{\mathrm{b}} + \mathbf{V}^{\phi} + \mathbf{V}^{\mathrm{f}}. \tag{25}$$

The contributions are: $\mathbf{V}^{\mathrm{s}}$—Biot-Savart integral given by formula (21); the potential field $\mathbf{V}^{\mathrm{b}}$ describes the deformation of vortices due to the presence of a stationary particle (on the particle surface $(\mathbf{V}^{\mathrm{s}} + \mathbf{V}^{\mathrm{b}}) \cdot \hat{\mathbf{n}} = 0$, where $\hat{\mathbf{n}}$ is the normal unit vector); $\mathbf{V}^{\phi} = \nabla\phi$ is the potential flow field induced by the motion of the spherical particle:

$$\phi(\mathbf{x}, t|\mathbf{r}_p) = -\frac{1}{2}\frac{a_p^3}{|\mathbf{x}-\mathbf{r}_p|^3}\mathbf{u}_p \cdot (\mathbf{x}-\mathbf{r}_p), \tag{26}$$

where $\mathbf{r}_p(t)$ is the current position of the particle center; the contribution $\mathbf{V}^{\mathrm{f}}$ is due to the mutual friction between the superfluid and the normal fluid:

$$\mathbf{V}^{\mathrm{f}} = h_{**}(\mathbf{V}^{\mathrm{s}} + \mathbf{V}^{\mathrm{b}} + \mathbf{V}^{\phi}) + h_{*}\mathbf{X}' \times (\mathbf{v}_n - \mathbf{V}^{\mathrm{s}} - \mathbf{V}^{\mathrm{b}} - \mathbf{V}^{\phi}) + h_{**}\mathbf{X}' \times (\mathbf{X}' \times \mathbf{v}_n). \tag{27}$$

These equations must be considered together with the equations of motion of neutrally buoyant spherical particle; these equations are $d\mathbf{r}_p/dt = \mathbf{u}_p(t)$, and

$$\frac{4}{3}\pi a_p^3 \rho_o \frac{d\mathbf{u}_p}{dt} = 6\pi a_p \mu_n (\mathbf{v}_n - \mathbf{u}_p) + 2\pi\rho_s a_p^3 \frac{\partial \mathbf{V}^{\mathrm{s}}(\mathbf{r}_p, t)}{\partial t} + \frac{1}{2}\rho_s \int_S dS |\mathbf{V}^{\mathrm{s}} + \mathbf{V}^{\mathrm{b}}|^2 \hat{\mathbf{n}}, \tag{28}$$

where ρ_o is given by the first of relations (13). At temperatures $1\ \mathrm{K} < T < T_\lambda = 2.17168\ \mathrm{K}$, $\mu_n(T)$ is the viscosity of the normal fluid. At $T < 1$ K, the coefficient μ_n is determined by the drag force due to ballistic scattering of quasiparticles (phonons and rotons) off the particle surface (see the discussion later in Sect. 3.3).

Note that the key difference between the one-way coupling model represented by (11)–(12) and the self-consistent, two-way coupling model considered in this section is the presence of the particle-vortex interaction force represented by the last term in the equation (28) of particle motion, the latter being coupled with equations (25)–(27) governing the evolution of the vortex filament.

Numerical method of solution of the system of equations (21) and (25)–(28) is described in detail by Kivotides, Barenghi, and Sergeev [39] (this method is based on generalization of the approach by Schwarz [35, 44], later developed further by Tsubota and Maekawa [45], to the problem of reconnection of the quantized vortex with the stationary surface or the surface moving with prescribed velocity).

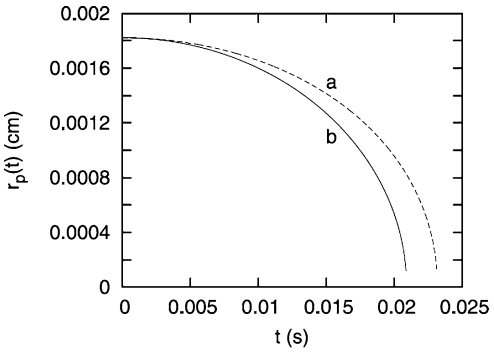

Fig. 14 Distance between the particle and the vortex core vs time: (**a**) one-way coupling model; (**b**) self-consistent two-way coupling model [40]. From Barenghi, Kivotides, and Sergeev, *J. Low Temp. Phys.* **148**, 293 (2007). Reprinted by permission, ©2007 Springer

Using this model we may analyze first how incorrect is the one-way coupling model. Figure 14 shows the distance between the particle and the initially straight vortex vs time found from (a) analytical calculation [18] based on the one-way coupling model, and (b) numerical, dynamically self-consistent, two-way coupling model [40] given by (21), (25)–(28). As can be seen, despite the simplicity of the one-way coupling model, agreement is good until the moment when the particle and the vortex are so close that the vortex reconnects to the particle surface.

3.2 Mechanism of Particle-Vortex Interaction

We will focus here only on the most important aspects of particle-vortex interaction, referring the interested reader to original publications of Kivotides, Barenghi, and Sergeev [33, 39–43].

All the calculations illustrated below were performed for the neutrally buoyant particle of radius $a_p = 1$ μm located initially at the distance $2a_p$ from the initially straight vortex filament. To simplify the analysis, in all examples considered below it was assumed that $\mathbf{v}_n \equiv \mathbf{0}$.

We illustrate first an influence of the initial velocity of solid particle on the particle-vortex collision [42]. Figure 15 shows a sequence of particle-vortex configurations at $T = 1.3$ K for initial velocity $u_p = 25$ cm/s. The particle arrives from the right; *top left*: the vortex is deformed as it tries to avoid the incoming particle; *top middle and top right*: the reconnection of vortex to the particle surface excites Kelvin waves; *bottom left*: the particle drags the vortex, forcing its two strands to come together, thus facilitating a second reconnection; *bottom middle*: following the reconnection, the vortex recoils and the particle breaks free; *bottom right*: the following relaxation creates more Kelvin waves.

The second computation is carried out at the same temperature for the smaller initial velocity $u_p = 20$ cm/s. In this case, illustrated by Fig. 16, the particle is trapped by the vortex: after reconnecting with the vortex the particle slows down and stops since it lacks the kinetic energy to stretch the vortex and to induce the second reconnection. Results illustrated by Figs. 15 and 16 indicate that, for each temperature, there exists a critical velocity, $v_{\rm cr}$ of the particle-vortex approach; provided the relative velocity of the particle and the vortex is smaller than $v_{\rm cr}$, the particle will be trapped on the quantized vortex core.

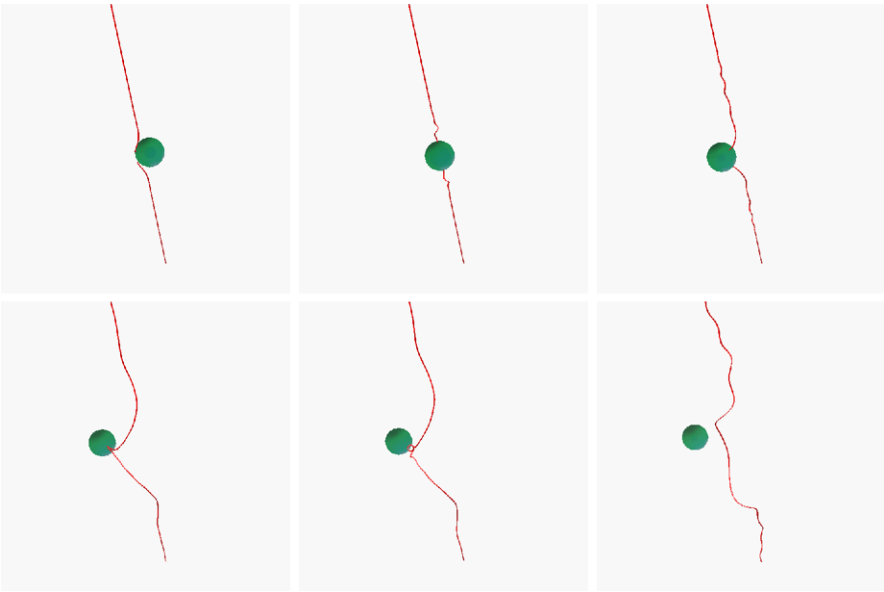

Fig. 15 (Color online) Particle-vortex collision [42] at $T = 1.3$ K. Initial velocity $u_p = 25$ cm/s. Particle moves from the right. From Kivotides, Barenghi, and Sergeev, *Phys. Rev. B* **77**, 014527 (2008). Reprinted by permission, ©2008 American Physical Society

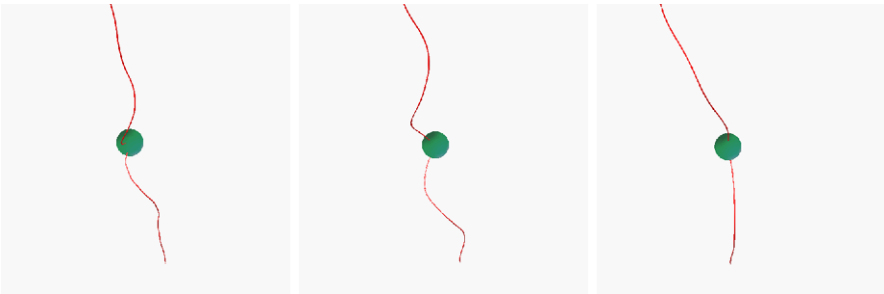

Fig. 16 (Color online) Particle trapping on the vortex core [42]. $T = 1.3$ K, initial velocity $u_p = 20$ cm/s. From Kivotides, Barenghi, and Sergeev, *Phys. Rev. B* **77**, 014527 (2008). Reprinted by permission, ©2008 American Physical Society

Note that in these two, somewhat artificial examples a possibility of nucleation of quantized vortices (and hence extra dissipation) by a moving particle has been ignored. A rather high particle velocities (20 and 25 cm/s) were used for the purpose of illustration only; similar results were obtained as well for considerably smaller velocities. It is unlikely that in the real turbulent ^{4}He the particle velocity relative to the vortex core can be as high as in these illustrations. For example, in the counterflow turbulence u_p can hardly be larger than v_{ns}, the latter usually being considerably smaller than the critical nucleation velocity.

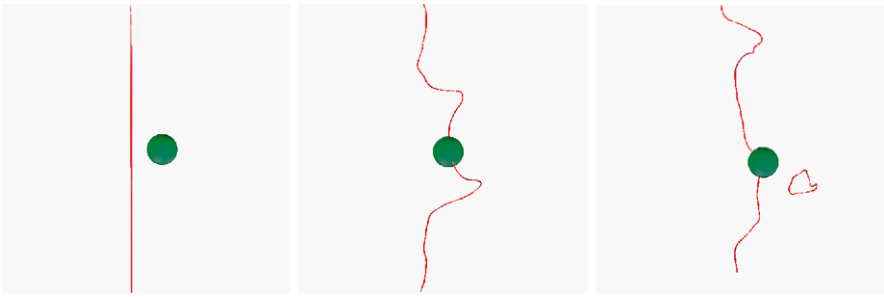

Fig. 17 (Color online) Particle trapping on the vortex core [33] at $T = 1.3$ K and $u_p = 0$. From Kivotides, Sergeev, and Barenghi, *Phys. Fluids* **20**, 055105 (2008). Reprinted by permission, ©2008 American Institute of Physics

It was also found [41] that having been trapped by the quantized vortex the particle may then drift along the vortex filament. For a neutrally buoyant, micron-size particle, a typical drift velocity, $v_{\rm drift}$ was found to be about 0.5 cm/s. Such a drift can be explained by the interaction of the particle with Kelvin waves (which are not necessarily symmetric with respect to the particle) induced by the particle-vortex collision. The drift velocity provides a rather simple way of estimating the amplitude of collision-induced Kelvin waves, e.g. by modeling a Kelvin wave of amplitude A as a vortex ring of radius A and then balancing the momentum of the ring with that of the drifting particle. For $v_{\rm drift} \approx 0.5$ cm/s such a procedure yields $A \approx 0.25$ μm.

3.3 Influence of Temperature on Particle-Vortex Collision and Particle Trapping

Another computation [33] was carried out at temperature $T = 1.3$ K for the particle initially at rest. The particle starts moving under the influence of the radial pressure gradient generated by the vortex. Figure 17 shows the sequence of particle-vortex configurations at times $t = 0$ (left), 0.125×10^{-2} s (center), and 0.263×10^{-2} s (right). The last frame shows that the vortex traps the particle and emits a small vortex ring (note that this feature is not common for all trapping events) thus reducing the total energy of the particle-vortex configuration. The results of calculation [33] for the same initial configuration and particle velocity, but μ_n assumed to be only 0.2 of its value at $T = 1.3$ K seem to suggest that at any, however small, non-zero initial velocity, the particle, although undergoing the process of reconnection with the vortex filament, eventually breaks free, so that trapping does not occur. Similar (in fact, almost identical) scenario is typical of $T \to 0$ limit when the (viscous) damping force acting on the particle can be neglected. (However, this issue is less trivial than it seems—see the discussion below.)

These examples show that the presence of the damping is crucial for trapping of solid particles by quantized vortices, so that it can be, rather naively, expected that trapping cannot occur at temperatures below 1 K when the normal fluid is absent. However, at $T < 1$ K there still exists a damping force, $\mathbf{F}^{\rm d} = -6\pi a_p \mu_n \mathbf{u}_p$ caused by ballistic scattering of quasiparticles (phonons and rotons) off the particle surface. Note the Stokesian form of this force (cf. (7), although $\mu_n(T)$ should now be understood not as a viscosity but as the damping coefficient).

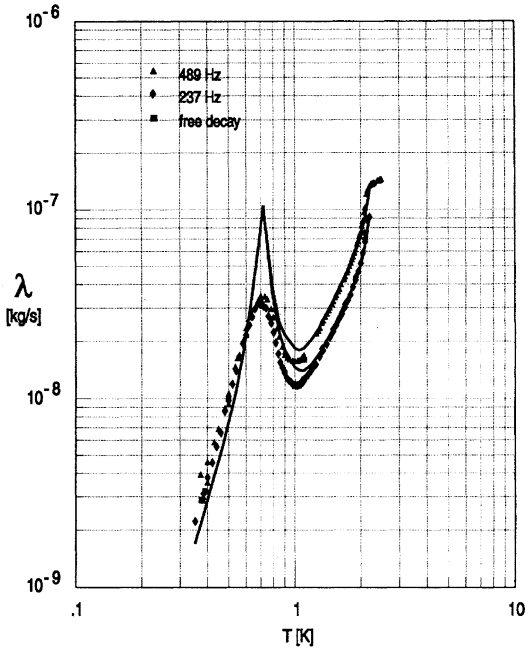

Fig. 18 Damping coefficient λ as a function of temperature [46] (experimental results of Jäger, Schuderer, and Schoepe, *Phys. Rev. Lett.* **74**, 566 (1995)). Reprinted by permission, ©1995 American Physical Society

Calculations [33] for various values of the damping coefficient showed that trapping does not occur in the case where the damping coefficient, μ_n is smaller than $0.2 \times \mu_n$ (1.3 K). The value of the damping coefficient was measured experimentally by Jäger, Schuderer, and Schoepe [46] for the spherical particle of radius 100 μm. Figure 18 shows the experimental results [46] for the coefficient $\lambda = 6\pi a_p \mu_n$ in the range of temperatures including both the region $T > 1$ K corresponding to the classical viscous dissipation in the normal fluid, and $T < 1$ K corresponding to the regime of ballistic scattering of quasiparticles. It can be seen that in the temperature interval $0.6\ \text{K} < T < 1\ \text{K}$ the value of μ_n may even exceed the viscosity at temperatures above 1 K. Only at temperatures below 0.5 K the damping coefficient becomes smaller than $0.2 \times \mu_n$ (1.3 K). Therefore, it can be expected that the trapping of neutrally buoyant, 1 μm particles does not occur at temperatures below 0.5 K.

At these, very low temperatures the motion of solid particle can be modeled by a simpler, one-way coupling model which is based on the assumption that particles are not trapped on quantized vortex lines. However, at these temperatures the presence and motion of the particles still affects the vortex filaments, so that a certain modification should be necessary of the one-way coupling model. Such a modification was already discussed above in Sect. 2.5.3.

It was already mentioned rather briefly that the results discussed above can be invalidated in the case where the extra dissipation is produced by the nucleation of quantized vortices in the vicinity of the particle whose velocity relative to the superfluid component is sufficiently large. The details of this mechanism are not properly understood yet and require further, rather complicated numerical study. Perhaps the only example of such a study so far is the work of Hänninen, Tsubota, and Vinen [47] who hinted at the possibility of formation of a wake, growing with time, of quantized

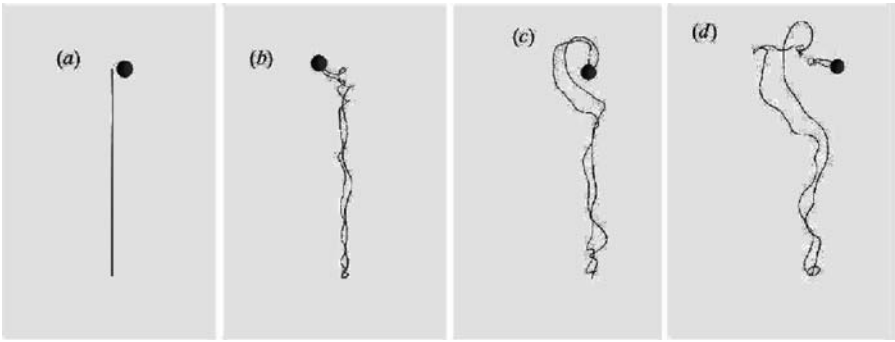

Fig. 19 Example [31] of the particle-vortex interaction at $T = 0$. Initial radius and velocity of the ring are $R = 1.25 \times 10^{-3}$ cm and $V_R = 0.771$ cm/s. The particle is initially at rest. Four frames, from *left* to *right*, correspond to times $t = 0$, 3.407×10^{-4}, 5.679×10^{-4}, and 7.698×10^{-4} s. From Kivotides and Wilkin, *J. Fluid Mech.* **605**, 367–387 (2008). ©2008 Cambridge University Press

vorticity behind an oscillating sphere. However, we anticipate that relatively small particle velocities typical of PIV or particle tracking experiments allow to ignore the extra dissipation due to the nucleation of quantized vortices.

3.4 Self-consistent Model of Particle Collisions with Vortex Rings

The self-consistent, two-way coupling model described in this section, was recently applied by Kivotides and Wilkin [31] for numerical study of interactions between neutrally buoyant solid particles and quantized vortex rings in the range of temperatures between $T = 0$ and $T = T_\lambda$. It was found that trapping of particles by sufficiently small vortex rings never occurs, and that, at $T = 0$, the dominant dynamical process in the particle-ring interaction is the excitation and propagation of Kelvin waves along the vortex ring. The collision between the particle initially at rest and the vortex ring of radius 1.25×10^{-3} cm at temperature $T = 0$ is illustrated by the sequence shown in Fig. 19. It was found that typical of the particle-vortex collisions at $T = 0$ is spiraling of the particle out of the point of initial contact with the vortex ring. At finite temperatures the particle-vortex collision induces particle oscillations in the direction normal to the particle trajectory. As should be expected, at finite temperatures the mutual friction damps the amplitude and reduces the frequency of Kelvin waves propagating along the ring.

4 Visualization Experiments and Their Theoretical Interpretation

4.1 Particle Motion in Turbulent Thermal Counterflow

4.1.1 Experiment

One of the first and, in our view, one of the most important experiments illustrating strong interactions between solid particles and quantized vortices was performed by

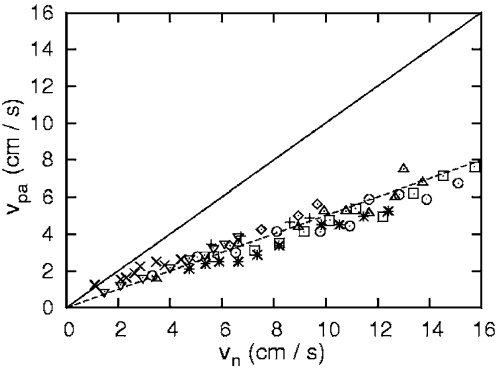

Fig. 20 PIV measurement of Zhang and Van Sciver [5] of $v_{\rm pa} = u_p + v_{\rm slip}$ for particles sedimenting in turbulent thermal counterflow. *Solid line*: $v_{\rm pa}$ calculated according to (29) and (30); *dashed line* is calculated [22] from (34) and (35) with $\beta = 3$. Reprinted, by permission, from Sergeev, Barenghi, and Kivotides, *Phys. Rev. B* **74**, 184506 (2006). ©2006 American Physical Society

Zhang and Van Sciver [5] who studied the sedimentation of heavy ($\rho_p = 1.1$ g/cm^3) particles in thermal counterflow produced by the heat source situated at the bottom of vertical apparatus, so that the normal fluid flows upwards. The experiments were performed in the temperature range from 1.62 to 2.0 K; the applied heat flux ranged from 110 to 1370 mW/cm^2.

It seemed natural to expect that the dominating force acting on the particle will be the viscous drag force and, therefore, the particle velocity will be

$$u_p = v_n - v_{\rm slip}, \tag{29}$$

where $v_{\rm slip}$ is the terminal velocity of particle sedimentation given by relation

$$v_{\rm slip} = \frac{2a_p^2}{9\mu_n}(\rho_p - \rho). \tag{30}$$

Were this correct, the experimental data for $v_{\rm pa} = u_p + v_{\rm slip}$ plotted against v_n would have collapsed on the straight solid line shown in Fig. 20. However, as can be seen from Fig. 20, the results of PIV measurement showed much lower particle velocity. Zhang and Van Sciver [5] found that, instead of (30), the particle velocity can be represented as $u_p = v_n - v_{\rm slip} - v_{\rm add}$, where the additional velocity, $v_{\rm add}$ can be explained only by strong interactions between sedimenting particles and the vortex tangle. Zhang and Van Sciver also found that $v_{\rm pa}/v_n \approx 0.5$ independently of temperature, and $v_{\rm add} \sim q = \rho S T v_n$.

4.1.2 Phenomenological Theory of Particle Motion

Below we will discuss the phenomenological theory, developed by Sergeev, Barenghi and Kivotides [22], of the motion of micron-size particles in thermal counterflow and hence explain the surprising result of Zhang and Van Sciver's experiment. The relatively simple analytical model of Sergeev, Barenghi and Kivotides arises from the physical insight acquired using the numerical (and computationally expensive) two-way coupling model.

Imagine that two strands of the quantized vortex are attached to the surface of spherical particle as shown in Fig. 3 (left) (at the point of reconnection the vortex

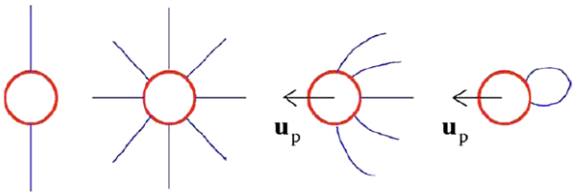

Fig. 21 (Color online) Possible particle-vortex configurations [22]. From Sergeev, Barenghi, and Kivotides, *Phys. Rev. B* **75**, 019904(E) (2007). Reprinted by permission, ©2007 American Physical Society

strand is necessarily orthogonal to the particle surface). The force exerted by a vortex strand attached to the surface is $\mathbf{F} = \int_S p\hat{\mathbf{n}}\,dS$ which, as shown by Schwarz [44], can be written as

$$\mathbf{F} = \frac{\rho_s}{2}\int_S |\mathbf{V}^{\mathrm{s}} + \mathbf{V}^{\mathrm{b}}|^2\hat{\mathbf{n}}\,dS. \tag{31}$$

The contribution of $\mathbf{V}^{\mathrm{b}}$ to this force can be neglected in the case where the radius of curvature of the vortex strand is much larger than the particle radius.

The vortex tangle in the counterflow can be so dense that several vortex strand can be simultaneously attached to the particle. Since the quantum of circulation is small, the leading contribution to the integral (31) is provided by a small area around the point where the vortex attaches to the surface. This enables us to find the following analytic approximation for the force exerted on the particle:

$$\mathbf{F} \approx \frac{\rho_s\kappa^2}{4\pi}\ln\frac{a_p}{\xi}\sum_{i=1}^{N}\hat{\mathbf{n}}_i. \tag{32}$$

It can be noticed that, in agreement with the experimental results [5], $\mathbf{F}$ is a body force.

Several possible particle-vortex configurations shown in Fig. 21 can be imagined. If configuration is symmetric, as in the first two figures, the net force is zero. If one or more vortex loops are asymmetrically attached to the sphere, as in the third and the fourth figures, the contributions from individual vortices will not cancel out resulting in a net body force.

The following scenario seems realistic: the sphere, as it moves between vortex lines, carries along one or more vortex lines or even separate loops as the result of previous close encounter with vortices. This scenario corresponds to asymmetric particle-vortex configurations, shown in Fig. 21, leading to emergence of the force exerted on the particle in the direction opposite to its motion. In the case of moderately dense tangle ($a_p \lesssim \ell$) typical of the experiment of Zhang and Van Sciver [5], the average force exerted on the particle by the vortex tangle can be calculated [22] as

$$F \approx \frac{\rho_s\kappa^2}{4\pi}\left(\frac{2\beta a_p}{\ell}\right)\ln\frac{a_p}{\xi}. \tag{33}$$

Here the only unknown quantity is the parameter β which should be determined by geometrical properties of the vortex tangle in the vicinity of the particle. It can be expected that $\beta = O(1)$.

The additional velocity can now be calculated as $v_{\rm add} = F/(6\pi a_p \mu_n)$, so that for $v_{\rm pa} = u_p + v_{\rm slip}$ we find

$$v_{\rm pa} = v_n - v_{\rm add} \approx \left(1 - \frac{\beta\rho\kappa^2\gamma \ln(a_p/\xi)}{12\pi^2\mu_n}\right) v_n, \tag{34}$$

where $\gamma(T) = L^{1/2}/v_{ns} = \rho_s L^{1/2}/(\rho v_n)$ is the known mutual friction coefficient, with $v_{ns} = v_n - v_s$. In agreement with the experimental results [5] we find that $v_{\rm pa}$ is proportional to the normal fluid velocity. Moreover, the temperature dependence of the slope $v_{\rm pa}/v_n$ turns out to be the same as in the cited experiment.

Using formula (34), the ratio of the additional velocity to the heat flux can be calculated as a function of temperature:

$$\frac{v_{\rm add}}{q} = \frac{\beta\kappa^2 \ln(a_p/\xi)}{12\pi^2} \left(\frac{\gamma}{\mu_n ST}\right), \tag{35}$$

so that $v_{\rm pa}$ can now be calculated explicitly. The dashed line in Fig. 20 reproduces $v_{\rm pa}$ calculated by Sergeev, Barenghi, and Kivotides [22] using formulae (34)–(35) with $\beta = 3$. As can be seen, the developed phenomenological theory agrees well, not only qualitatively but also quantitatively, with PIV measurements of Zhang and Van Sciver and, therefore, seems to explain the mechanism of particle motion in the thermal counterflow.

Calculations similar to those leading to formulae (33)–(35) can also be performed in the limit of the very dense vortex tangle such that $a_p \gg \ell$. In this case reconnections between the particle and vortices happen all the time, so that the particle is always attached to several vortex filaments. Calculation of the average force exerted on the particle by the vortex tangle yields [22]:

$$F \approx \frac{\rho_s\kappa^2}{4\pi} 2\beta_d \left(\frac{a_p}{\ell}\right)^2 \ln\frac{a_p}{\xi}, \tag{36}$$

where $\beta_d = O(1)$ is again a geometrical factor, and $(a_p/\ell)^2$ represents the cross-section of the particle interaction with the network of vortices. Proceeding as in the previous case, a different (cf. (34)) dependence of $v_{\rm pa}$ on v_n, T and a_p is predicted:

$$v_{\rm pa} \approx v_n \left[1 - \frac{\beta_d a_p (\kappa\gamma\rho)^2 \ln(a_p/\xi)}{12\pi^2\mu_n\rho_s f} v_n\right], \tag{37}$$

where $f = 1 + \beta_d\gamma/(3\pi\mu_n)$. Finding whether or not this prediction agrees with observations would require a new experiment similar to that of Zhang and Van Sciver [5] but for considerably higher values of the vortex line density (i.e. such that $L \gg a_p^{-2}$).

4.1.3 Self-consistent Model of Particle Motion in the Thermal Counterflow

In order to justify the phenomenological theory of Sect. 4.1.2 and investigate the particle motion in more detail, Kivotides [48, 49] applied the two-way coupling, self-consistent model described in Sect. 3.1 for a numerical study of particle interactions

with the vortex tangle in thermal counterflow. Although in the cited works the motion of not a heavy but neutrally buoyant particle was studied, the results reveal some important aspects of the experiments performed by Zhang and Van Sciver [5] and Paoletti et al. [10].

We start this section with reviewing the first of these papers. In calculations [48] the normal fluid velocity in the counterflow was assumed a constant, prescribed value (this was the only realistic option considering the complexity of the model represented by (25)–(28)). Numerical analysis of the particle motion was performed for the statistically steady vortex tangle modeled in the same way as in the earlier work [32] described in Sect. 2.5.2.

Calculations were performed for three temperatures, $T = 1.3$, 1.95, and 2.171 K. It was found that the following four factors strongly affect the particle motion: (1) stratification of the vortex tangle, (2) vortex line density, (3) the average drift of the tangle, and (4) the intensity of Kelvin wave cascades, induced by particle-vortex collisions, along vortex filaments. For example, for $T = 1.95$ K Kivotides found that the tangle is strongly stratified, and an average drift of the tangle is small. Since the vortices expand mostly in the direction normal to that of the counterflow, it was also found that in the considered case the stratification does not affect the average properties of the particle motion. The statistically steady particle motion is governed by the balance of the Stokes force acting in the direction of the normal flow, and the average particle-vortex interaction force acting in the opposite direction; the latter force was found to be proportional to the vortex line density and the mean relative particle-tangle velocity.

The calculations [48] confirmed the mechanism suggested by the phenomenological theory [22] discussed in the previous section: a formation of vortex loops attached to the rear part of the particle surface causes an additional force opposite to the direction of particle motion and hence reduces the slip velocity. For $T = 1.95$ K and the vortex line density $L = 3.284 \times 10^7$ cm^{-2} Kivotides' calculation yielded $\langle u_p \rangle \approx 0.6 v_n$, in a very good agreement with experimental results of Zhang and Van Sciver [5].

At the same temperature but higher vortex line density, $L = 8.284 \times 10^7$ cm^{-2} Kivotides found that the "head-on" particle-vortex collisions are more important and counterbalance the force caused by the formation of vortex loops in the rear part of the particle, so that $\langle u_p \rangle \approx v_n$. It was also found that the drift of the tangle in the direction opposite to the particle velocity increases the frequency of the "head-on" particle-vortex collisions and hence the average particle velocity. This effect becomes more pronounced at higher temperature; thus, for $T = 2.171$ K and $L = 5.846 \times 10^7$ cm^{-2} it was found that $\langle u_p \rangle \approx 1.2 v_n$, again in a very good agreement with experimental results [5].

At lower temperature, $T = 1.3$ K, Kelvin waves generated by particle-vortex collisions decay slower than at higher temperatures. This, in turn, leads to large amplitudes of particle velocity fluctuations which become comparable with $\langle u_p \rangle$. The intensity of these fluctuations was found to be inversely proportional to the temperature and the average velocity of the tangle drift relatively to the particle.

As argued in Sect. 3.2 (for details see original publications of Kivotides, Barenghi, and Sergeev [39, 42]), at 0.5 K $< T < T_\lambda$ there should exist a critical velocity of the

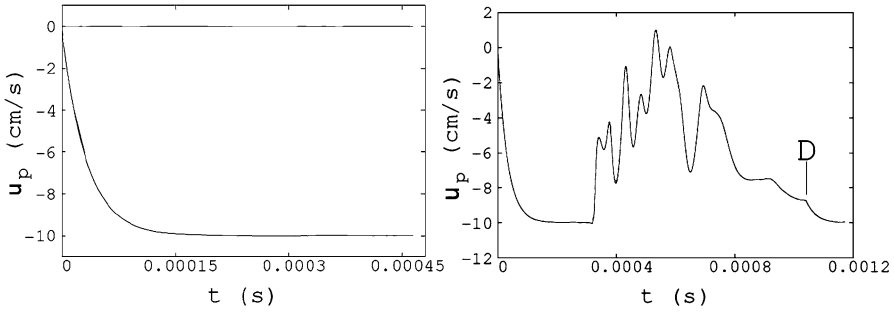

Fig. 22 *Left*: particle velocity vs time in the absence of particle-vortex collisions (the transition part of the curve corresponds to the particle response time). *Right*: u_p vs time illustrating the particle-vortex collision; D indicates the moment when the vortex detaches from the particle surface and the particle velocity starts adjusting to the normal flow [49]. Adapted from Kivotides, *Phys. Rev. B* **78**, 224501 (2008). By permission, ©2008 American Physical Society

particle-vortex approach below which a neutrally buoyant particle will necessarily be trapped by the initially straight quantized vortex. Kivotides noted [49] that at high counterflow velocities the tangle is very dense and, therefore, particle-vortex interactions become so strong that it may no longer be possible to measure the normal velocity. In the cited work he estimated the parameters of counterflow in which the normal velocity would be above the trapping limit but yet sufficiently low, such that the tangle is sufficiently dilute to enable the measurement of the normal velocity by the PIV or the particle tracking technique.

Using the same model as in his previous work [48], Kivotides [49] analyzed numerically, at temperature $T = 1.3$K, the particle motion in the thermal counterflow with the normal velocity $v_n = 10$ cm/s and the vortex line density $L = 1.168 \times 10^6$ cm^{-2}. Performing calculations for different initial positions of the particle, Kivotides found that in more than 50% of realizations the particle moved through the computational domain without experiencing any collision with the vortex tangle. On average, the deviation, caused by particle-vortex collisions, of the particle velocity from that of the normal fluid was found to be less than 4%. Moreover, in the case where the particle does not follow the normal fluid it tracks the motion of the vortex tangle. On the time series of particle velocity the events of the particle-vortex collision can be identified by strong oscillations (Fig. 22 (right), cf. the left frame showing the velocity of the particle moving through the tangle without collisions with quantized vortices) which can be filtered out to restore the normal velocity.

4.1.4 Particle Tracking Experiments

Another important visualization experiments in thermal counterflow are those by Paoletti, Fiorito, Sreenivasan, and Lathrop [10]. In contrast with the PIV technique, which analyzes the local average properties of the particulate flow, the particle tracking technique investigates individual particle trajectories. Experiments [10] were performed in the vertical apparatus with the heater at the bottom. The temperature and the applied heat flux, q ranged from 1.8 to 2.15 K and from 13 to 91 mW/cm^2, respectively (cf. the experiment of Zhang and Van Sciver [5] with q between 110

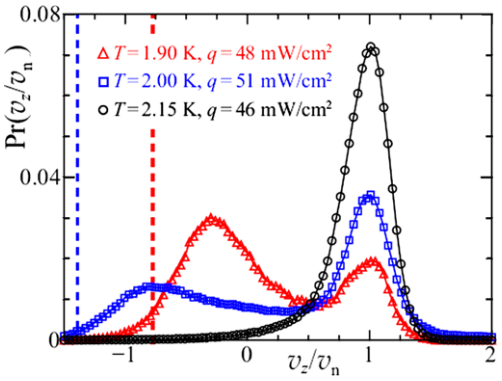

Fig. 23 (Color online) PDFs [10] of the particle velocity component in the direction of counterflow. After Paoletti, Fiorito, Sreenivasan, and Lathrop, *J. Phys. Soc. Jpn.* **77**, 111007 (2008). Reprinted by permission, ©2008 Physical Society of Japan

and 1370 mW/cm^2). Tracers were solid, micron-size hydrogen particles of density slightly smaller than that of liquid helium.

It was found that two distinct types of particle trajectories can be identified: (1) smooth trajectories corresponding to particles moving upward in the direction of the normal flow, and (2) irregular trajectories of particles moving downward; the latter trajectories were those of particles trapped on quantized vortices. Experimental observations [10] seem to confirm the earlier theoretical results [42] (see above Sect. 3.2) that at sufficiently low relative velocities between the normal fluid and quantized vortices the particles should be trapped more easily by the vortex tangle; at high relative velocities, although the particles interact with the tangle, it is unlikely that they become permanently trapped on the vortex lines.

Calculated from the experimental data [10], the probability distribution function (PDF) of the velocity component in the direction of the counterflow is bimodal, see Fig. 23, with the right peak at the normal fluid velocity, and the left, much broader peak corresponding to particles trapped by the vortex tangle. Note that, as would be expected, the fraction of particles trapped by the tangle and hence bimodality of the PDF disappear either with increasing temperature at constant heat flux (so that the vortex line density becomes smaller), or with increasing heat flux at constant temperature (so that v_n becomes sufficiently high to prevent particle trapping on quantized vortices).

Discussing these experimental findings, Paoletti et al. [10] claimed that their results do not agree with observations of Zhang and Van Sciver [5] who found that the particle velocity is proportional to the normal velocity, $u_p \approx 0.5 v_n$ independently of temperature. The authors [10] attributed this discrepancy to Zhang and Van Sciver's PIV technique which measures the local average properties of the particulate flow, while the technique employed by Paoletti et al. tracks the motion of individual particles. Paoletti et al. also stressed that their interpretation of experimental results differs significantly from the theoretical explanation of Sergeev, Barenghi, and Kivotides [22] (see also Sect. 4.1.2 above) whose underlying assumption was that every particle is affected by quantized vortices as it moves through the tangle, while the experimental observations [10] showed that there is a significant fraction of particles which move freely through the tangle without experiencing particle-vortex collisions. Furthermore, Paoletti et al. observed a significant temperature dependence of the par-

ticle motion, while the experiment [5] of Zhang and Van Sciver and the phenomenological theory [22] of Sergeev, Barenghi, and Kivotides both show that the disparity between the particle velocity and v_n is practically independent of temperature.

Below we will argue that the contradiction between the experimental results of Zhang and Van Sciver [5] and Paoletti et al. [10], as well as between theoretical interpretations of these results by Sergeev et al. and Paoletti et al. is only apparent. In fact, it seems that two recently published works by Kivotides [48, 49], reviewed in Sect. 4.1.3, already resolve this apparent contradiction. In these works, based on the two-way coupling, self-consistent (practically "first-principle") approach, Kivotides has shown that there exist two distinct regimes of particle motion, one corresponding to a relatively dense, and another to a relatively dilute vortex tangle. In the first of these publications Kivotides found that in the case where the vortex tangle is sufficiently dense ($L = 3.284 \times 10^7$ cm^{-2} corresponding to the intervortex spacing $\ell \approx 1.7$ μm in the considered example [48]) the average particle velocity is $0.6v_n$ in a very good agreement with the experimental results of Zhang and Van Sciver [5]. Kivotides also showed that in the considered case the particle is permanently affected by quantized vortices as it moves through the tangle, and that the mechanism of particle-vortex interactions agrees with that suggested by the phenomenological model of Sergeev, Barenghi, and Kivotides [22]. On the other hand, in the second of his publications [49] Kivotides, having analyzed numerically a particle motion in a more dilute tangle ($L = 1.168 \times 10^6$ cm^{-2}, $\ell \approx 9$ μm), found that in more than half realizations the particle moves through the tangle with the normal fluid without interacting with vortices. In the remaining less than 50% realizations he observed strong particle-vortex interactions which in most cases can be described as trapping-untrapping events. Were it calculated based on the results reported in the second of his publications [49], the PDF would have the same bimodal shape as found experimentally by Paoletti et al. [10].

Although, in terms of the heat flux, the regimes of counterflow in two reviewed experiments were adjacent, in most observations of Zhang and Van Sciver the heat flux was an order of magnitude or more higher than that in the experiments of Paoletti et al. This means that, at the same temperature (e.g. 1.95 K in both experiments), the intervortex spacing in the experiments of Zhang and Van Sciver ($\ell \approx 6$ μm with 1.7 μm particle in a typical experiment) was at least an order of magnitude smaller than in the reviewed experiment of Paoletti et al. Therefore it can be argued that two reviewed experimental observations do not contradict each other but simply correspond to two distinct regimes of particle motion. The parameter defining each of these regimes is the ratio of the particle size to the intervortex spacing, a_p/ℓ.

As far as the issue of temperature independence of the factor k in the relation $\langle u_p \rangle \approx k v_n$ is concerned, Zhang and Van Sciver's results [5] are not truly temperature independent: a closer inspection reveals a relatively weak dependence of k on temperature (the value $k \approx 0.5$ was obtained by averaging of a large number of experimental data). Likewise, in the phenomenological theory developed by Sergeev, Barenghi, and Kivotides [22] this factor is only approximately temperature independent being a function of the mutual friction coefficient γ and of the parameter β which, characterizing the geometry of interactions between the tangle and the particle, is itself temperature-dependent.

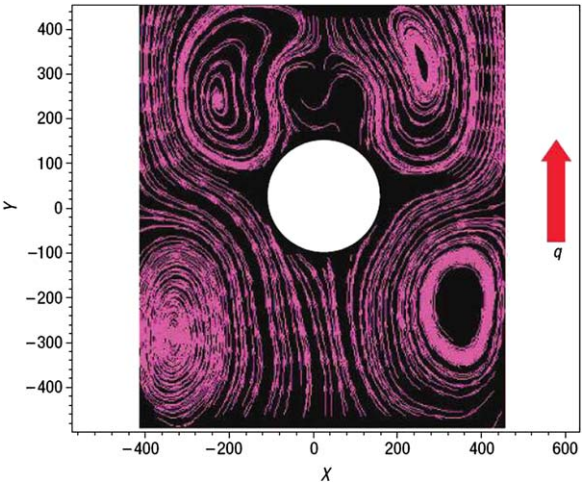

Fig. 24 (Color online) Streamlines of the particulate motion in the counterflow around the cylinder [6] ($q = 1.12$ W/cm^2, $T = 2.03$ K). From Zhang and Van Sciver, *Nature Physics* **1**, 36 (2005). Reprinted by permission, ©2005 Macmillan Publishers Ltd.

4.1.5 PIV Experiment in Thermal Counterflow with Cylindrical Obstacle

Among surprising experimental results obtained by the PIV technique is the recent observation by Zhang and Van Sciver [6] of the apparently stationary normal fluid eddies in the thermal counterflow past a cylinder. In the cited work, Zhang and Van Sciver visualized the motion of small particles in the thermal counterflow around the cylinder of diameter $D = 0.635$ cm fixed in the center of rectangular channel of a cross-section 3.89×1.95 cm^2. The counterflow was produced, in two separate experiments, by the heat flux $q = 0.4$ and 1.12 W/cm^2 at temperatures $T = 1.6$ and 2.03 K, respectively (corresponding to the Reynolds numbers $\mathrm{Re} = \rho D v_n/\mu_n = 4.1 \times 10^4$ and 2.1×10^4). Solid particles used for visualization in the PIV experiments were polymer microspheres of diameter 1.7 μm and density 1.1 g/cm^3. In these experiments Zhang and Van Sciver observed the formation of large-scale eddies of the particulate motion located both downstream and, surprisingly, upstream of the cylinder with respect to the normal flow. These, apparently stable vortices of the particulate flow field were located at distances about 3 cylinder radii from its center at the angles $\pm 45°$ and $\pm 135°$ to the axis along the undisturbed flow through the center of the cylinder, see Fig. 24. Note that the observed flow structures do not have a classical analogue.

Zhang and Van Sciver attributed the existence of apparently stationary normal eddies to the mutual friction interaction between quantized vortices and the normal fluid. However, our recent study [50] showed that perhaps the experimental results [6] can be interpreted without invoking the mechanism of interaction between the normal fluid and quantized vortices. Indeed, the calculation of motion of point vortices in the imposed potential flow around the circular disk shows that there exist stationary locations of point vortices, both at the rear and at the front of the disk. These locations are unstable: any perturbation of the initial stationary positions of point vortices leads, eventually, to sweeping of point vortices away from their initial locations. Furthermore, some of these stationary locations are positioned practically as the eddies seen by Zhang and Van Sciver. The point vortices in the vicinity of such positions

will remain close to their initial locations during the time period corresponding to the duration of the experiment [6] and hence seen as apparently stable.

Although this, purely classical explanation of the apparent stability of vortex structures does not invoke any interaction between the normal and the superfluid components of ^{4}He, the emergence of eddies seen in the experiment [6] might still require an explanation based on the analysis of mutual friction between quantized vortices and the normal fluid.

5 ^{4}He Channel Flow and Turbulent Boundary Layer

This short section describes the recent experiment which might be a beginning of systematic study of nonuniform ^{4}He flows. Xu and Van Sciver [51] reported the PIV measurements, using micron-size deuterium particles, of the ^{4}He forced flow in the rectangular channel for the normal fluid Reynolds numbers ranging from 9×10^4 to 4.5×10^5 and temperatures from 1.65 to 2.10 K. In this experiment, at scales larger than the intervortex spacing, the normal and superfluid components of ^{4}He can be considered as fully interlocked so that the measurements of the particulate velocity field yield an unambiguous velocity profile of the fluid. The results of Xu and Van Sciver's measurements were summarized in two graphs [51] shown in Fig. 25.

Xu and Van Sciver concluded [51] that in the wall region the velocity distribution agrees reasonably well with the classical nth-power law (for n ranging from 7 to 8.8). They also addressed the following questions which yet to be answered. Why the velocity profile is wider and flatter than that in the classical viscous channel flow? What is the nature of dependence on Reynolds number of the results shown in Fig. 25 (left)? Why, as seen from Fig. 25 (right), the normal fluid density does not seem to affect the shape of velocity profiles?

6 Visualization of Vortex Reconnections. Velocity Statistics in Decaying Quantum Turbulence

In a recent experiment [9] Bewley, Paoletti, Sreenivasan, and Lathrop observed the motion of solid hydrogen particles trapped on quantized vortices. The specific purpose of this work was a direct experimental investigation of vortex reconnections in turbulent ^{4}He. A sequence of images [9] illustrating the motion of particles trapped on vortex filaments is reproduced in Fig. 26.

To quantify their results, Bewley et al. [9] assumed that the evolution of reconnecting vortices can be characterized by a single scale parameter, $l(t)$. Using, as a measure of $l(t)$, the experimentally observed distance between two particles closest to the point of reconnection, they found that the evolution obeys the scaling $l \sim (t - t_0)^{1/2}$, where t_0 corresponds to the moment of reconnection of two vortices.

The particle tracking technique was further developed by Paoletti, Fisher, Sreenivasan, and Lathrop [11] to investigate, by analyzing the trajectories of tracer particles, the velocity statistics in decaying quantum turbulence. The decay of turbulence produced initially by the thermal counterflow was studied after the counterflow has been

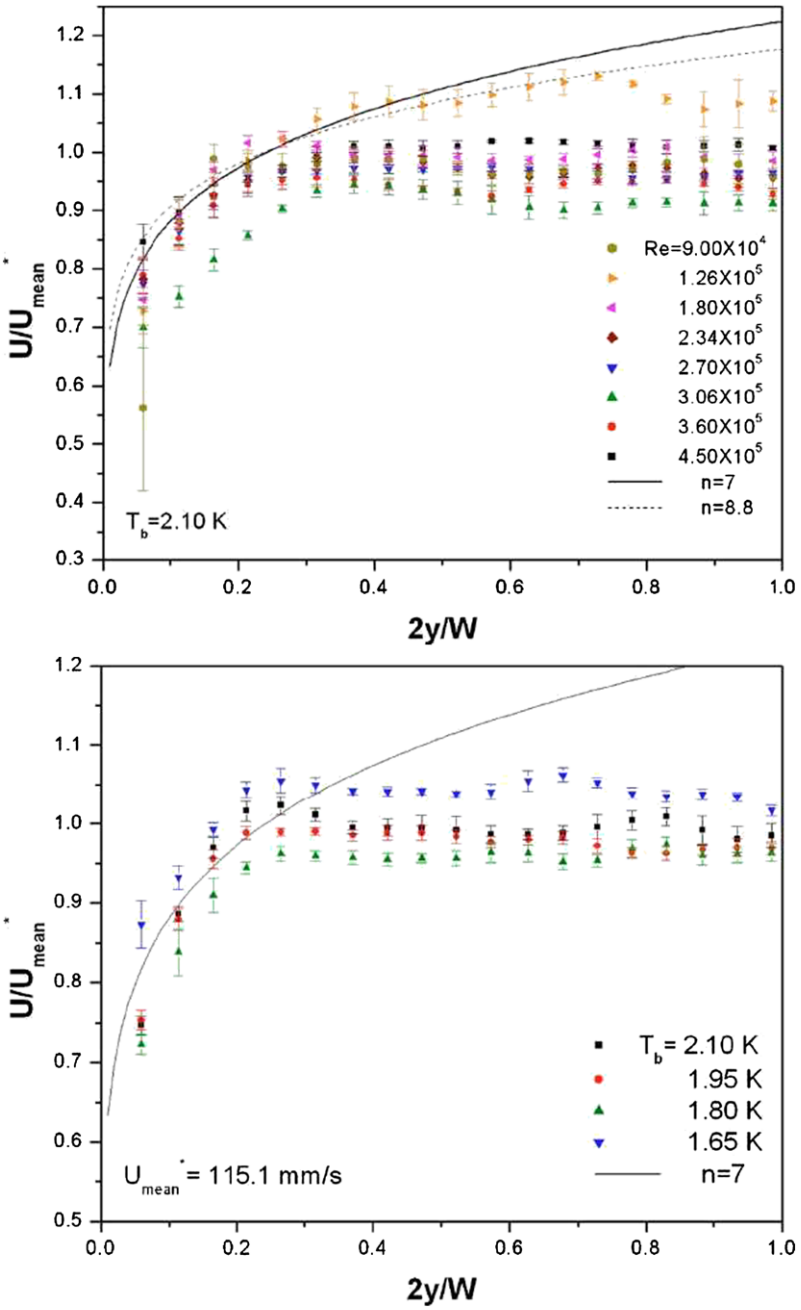

Fig. 25 (Color online) Normalized velocity profile [51] for different Reynolds numbers at $T = 2.10$ K (*top*), and at different temperatures for the mean velocity $U_{\text{mean}}* = 11.5$ cm/s (*bottom*); W is the width of the square channel. From Xu and Van Sciver, *Phys. Fluids* **19**, 071703 (2007). Reprinted by permission, ©2007 American Institute of Physics

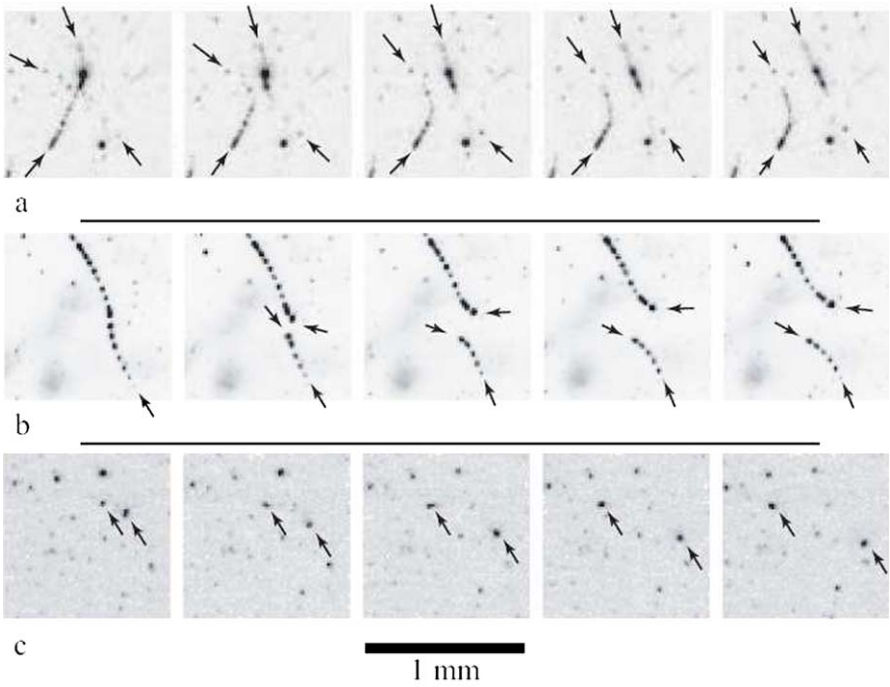

Fig. 26 (Color online) After Bewley, Paoletti, Sreenivasan, and Lathrop (*Proc. Nat. Acad. Sci.* **105**, 13707 (2008)): visualization [9] of the vortex dynamics. The particles trapped on quantized vortices can be easily identified. In each of the sequences (**a**), (**b**), and (**c**), the images were taken at 50 ms intervals. (**a**) Two approaching vortices have several particles trapped on their filaments (the first frame shows the projection in which the vortices appear crossed). The sequence (**b**) seems to show the vortices moving apart after the reconnection. The sequence (**c**) illustrate the authors' [9] method of identification of reconnecting vortices by a sudden motion of two tracer particles away from each other. ©2008 USA National Academy of Sciences

stopped by switching the heater off. Paoletti et al. found that the PDF of the particle velocity is strongly non-Gaussian with a pronounced tail obeying v^{-3} power law, see Fig. 27. The authors attributed such a tail to high velocities produced by reconnections of quantized vortices. The experiment has stimulated calculations [52] of turbulent velocity statistics in the context of three-dimensional and two-dimensional atomic Bose-Einstein condensates; after finding similar non-Gaussian velocity statistics in these related quantum systems the authors argued that, in general, non-Gaussian statistics arise from the singular nature of the velocity field around quantized vortices.

The results of fundamental importance reported in these two reviewed publications [9, 11] raise, however, the following question: what effect have the particles trapped on vortex filaments on the evolution of quantized vortices and, in particular, on the reconnection of two approaching vortices? In their work [10] reviewed earlier in Sect. 4.1.4 the authors claimed that, because in their experiments the distance between micron-size particles trapped on the same vortex filament was typically about 100 μm, the influence of trapped particles on the evolution of vortices can be ne-

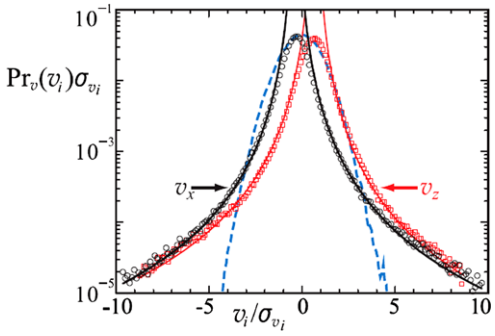

Fig. 27 (Color online) Probability distribution functions [11] of the velocity components in the direction of (v_z) and normal to (v_x) the counterflow. The distributions are scaled with $\sigma_{v_z} = 0.074$ cm/s and $\sigma_{v_x} = 0.066$ cm/s, respectively. The *dashed* (*blue*) *line*—velocity PDF, scaled with $\sigma_v = 0.25$ cm/s, for classical turbulence. From Paoletti, Fisher, Sreenivasan, and Lathrop, *Phys. Rev. Lett.* **101**, 154501 (2008). Reprinted by permission, ©2008 American Physical Society

glected. This claim is yet to be justified (especially where the motion and evolution of vortex filaments near the reconnection point is concerned). It is unlikely that at present this problem can be treated experimentally; a more realistic alternative seems to be a development of the mathematical model of a vortex filament loaded by trapped solid particles [53].

7 Related Techniques: Detection of Vortices by Trapping of Negative Ions and Imaging of He_2 Molecules

7.1 Ion Trapping

The technique of vortex detection by ion trapping was recently reviewed in a number of regular research publications including some in this journal [54, 55], so that we will present here a rather brief overview of theoretical and experimental aspects of this technique.

The idea of using charge carriers for detection of quantized vortices in superfluids is much older than that of using solid particles for the flow visualization in ^{4}He and dates back to the works of Careri [56–59], and Reif and Meyer [60–62]. The technique is based on the phenomenon that a negative charge (a single electron) injected into ^{4}He self-localizes itself in a spherical void (known as the ion or electron bubble) of radius 12–20 Å (depending on pressure) from which helium atoms are excluded. (A relatively large size of this, almost macroscopic bubble justifies inclusion of this section into our review otherwise concerned with the motion of much larger, solid particles in ^{4}He.) The model of the negative ion bubble was proposed by Ferrel and later elaborated by Kuper and other authors [63–66] and confirmed experimentally by Levine and Sanders [67]. Consistent with the bubble model of the negative charge carrier is the effective mass of the ion, M^* determined in Refs. [68–70]. It appears in the Langevin equation of motion for the ion's drift velocity, $\mathbf{u}_D$ in the electric field,

$\mathbf{E}$: $e\mathbf{E} = M^*(d\mathbf{u}_D/dt + \mathbf{u}_D/\tau)$, where e is the electron charge, and τ the phenomenological relaxation time. The effective mass of the ion was found [68–70] to be of the order 100 masses of ^{4}He atom (in agreement with the bubble model), and τ appears to be the viscous relaxation time introduced above in Sect. 2.2. (The detailed treatment for the Stokes problem of the ion bubble motion, albeit in normal ^{4}He, was given by Ostermeier and Schwarz [71].)

The possibility of using negative ions as detectors (or "probe particles") of quantized vortices is due to the fact that the ion bubble is attracted to the vortex by the Bernoulli force. The combined action of the Bernoulli effect and the reduced condensation energy of the core produces a potential well of the depth of the order 50 K [72, 73] and hence traps the ion. This mechanism [72, 73] is practically identical to that described above in Sect. 2.3 of trapping of solid particles on the vortex cores. (Note that the mechanism of trapping of the ion bubble by the quantized vortex in ^{4}He modeled as the Bose condensate was studied by Berloff and Roberts [23] and described above in Sect. 2.3.2.)

The model of the positive charge carrier in ^{4}He was developed by Atkins [74] in 1959 and became since then commonly accepted. According to this model the positive ion exerts an electrostrictive attraction on the surrounding fluid thus causing a liquid-solid transition resulting in a core ("cluster" or "snowball") of solid helium. The radius of this snowball is from 7 to 9 Å, depending on pressure. Like the negative ion bubble, such a snowball will be attracted, by the Bernoulli force, to the vortex core so that, in principle, positive ions can also be used for detection of quantized vortices. However, a smaller than that of the ion bubble radius of the snowball and, therefore, the cross-section of the snowball-vortex interaction make the experimental technique using positive ions more difficult and less practical. Hence in this review we will discuss only works concerned with negative charge carriers.

The realization of the negative ion technique can be illustrated by the following arrangements of the experiment, typical of the early observations of single vortex lines in rotating ^{4}He: quantized vortex lines are charged first by ion bubbles trapped on them using e.g. the electron beam emitted orthogonally to the axis of rotation. The vortex lines are then detected by applying the electric field parallel to the axis of rotation so that trapped electron bubbles slide along vortex filaments to a collector attached to an electrometer. The latter registers the amount of collected charge which is proportional to the number of vortex lines present. In its early, simplest version this technique allowed to determine only the total number of (almost) straight quantized vortex lines in a slowly rotating container. Its subsequent modifications made possible also detection of individual vortex lines and later the measurement of the vortex line density in turbulent ^{4}He.

The theory of ion trapping by the quantized vortex has been developed in classical works of Donnelly, Roberts, and Parks [21, 75–77]. To analyze ion-vortex interactions, two competing mechanisms were taken into account: trapping of the ion bubble, moving in the electric field, in the potential well of the vortex, and escape of the trapped ion due to its Brownian motion, which was considered to be in equilibrium with thermal (quasiparticle) excitations in ^{4}He. Two parts of this problem were calculations of (1) the trapping (or capture) cross-section, σ, cm, and (2) the escape probability, P, s^{-1}; the second part was analyzed using Smoluchowski or Fokker-

Planck equations in the framework of the Kramers-Chandrasekhar method for calculation the probability of escape of a particle by diffusion from a potential well. The capture cross-section was found to be of the order 10^{-6} to 10^{-5} cm and to decrease with the electric field and increase with temperature to about 1.6 K, at which temperature it drops sharply. The escape probability (or, equivalently, the mean trapping lifetime, $t_\ell \sim P^{-1}$) was found in a good agreement with experimental data obtained by Springett, Tanner, and Donnelly [78–80] as well as with experimental results of Douglass and Cade [81, 82]. The effective cross-section can then be calculated as $\sigma_{\rm eff} = \sigma e^{-Pt}$, where t is some characteristic time. Parks and Donnelly [21] further developed the theory in order to make possible calculation of the ion bubble radius from the experimentally measured mean trapping lifetime. This required, in particular, a calculation of the so-called substitution energy, i.e. a kinetic energy of rotating superfluid excluded by the trapped bubble. For the ion bubble of radius R trapped symmetrically on the vortex core this was found as

$$\Delta E = \frac{\rho_s \kappa^2 R}{2\pi}\left[1 - \left(1 + \frac{\xi^2}{R^2}\right)^{1/2} \sinh^{-1}\left(\frac{R}{\xi}\right)\right] \tag{38}$$

(note that formula (18) of Sect. 2.3.1 follows from (38) assuming $R = a_p \gg \xi$). In the context of further experimental studies discussed below, it is worth noticing that the substitution energy (equal to the depth of the potential well) is about 50 K. Parks and Donnelly's study of bubble radii was further developed by Springett and Donnelly [83] who used the measurements of trapping cross-sections in the rotating container to deduce that the radius of the ion bubble decreases with pressure. The theory developed by Donnelly et al. also predicted that the mean trapping lifetime should increase with the superfluid density and with the radius of ion bubble. These predictions were soon confirmed experimentally by Springett [78] who measured, at various pressures and temperatures, the cross-section of the ion capture and ion mobilities in order to derive from these data the pressure and temperature dependence of the ion bubble radius and the mean trapping lifetime. Later Pratt and Zimmermann [84] also measured the mean trapping lifetime in the wide range of temperatures and pressures (from vaporization and solidification) and showed that at constant pressure the lifetime rapidly decreases with T. In particular, it was found [78] that at saturated vapor pressure trapping becomes negligible at temperature above 1.7 K, the value which is now often referred to as the "abrupt lifetime edge". It was also shown that the temperature, below which trapping becomes significant increases with pressure. Glaberson [85] measured the mobility, as a function of temperature and pressure, of negative ions trapped on quantized vortex lines, and arrived at the important conclusion that the negative ion bubbles do not deform as they are trapped on vortex cores. He also developed a new model, which appeared to account satisfactory for available experimental results, for the drag exerted on the trapped ion bubble, based on the assumption that the vortex line has several Å-thick central core surrounded by a tail of excess roton density with momenta opposite to the direction of circulation.

Among the first applications of the ion trapping technique for an investigation of vortex structures in ^{4}He was an observation by Northby and Donnelly [86] of a nonlinear dependence of the number of quantized vortex lines on the angular velocity of

the rotating container. This nonlinearity was found to be associated with the existence of a near-wall region, observed in the cited work, free of quantized vortices.

The early experiments [56–59, 87] have indicated that ions interact strongly with turbulence in ^{4}He, but no quantitative data have been obtained yet. The first experimental study of the turbulent vortex tangle by the ion trapping technique was undertaken by Sitton and Moss [88] in 1969 (in fact it was the first direct experimental confirmation that the turbulence in the superfluid component of ^{4}He is composed of individual, quantized vortex lines indistinguishable from those produced in the (slowly) rotating container except for their configurations). The vortex tangle was produced by the supercritical heat current at temperature above 1.6 K. Since most of the vortex lines are no longer straight but have a configuration of loops and kinks, the charge can no longer slide along the filaments to a collector but is trapped inside the tangle. The fraction f_Q of the trapped charge was measured and then linked with the vortex line density by the relation $f_Q = (1 + P/u_i \sigma L)^{-1}$, where u_i is the ion velocity, and L can be linked with the heat flux and properties of ^{4}He by the well known Vinen equation [89].

A series of experimental studies and their interpretation, beginning 1972 and spanning the period of nearly 30 years, was undertaken by the group led by Packard and Williams. In 1972, Packard and Sanders [90] showed the possibility of detecting individual vortex lines in rotating ^{4}He. The experiments were performed in a cylindrical container whose rotation slowly accelerated so that the number of vortex lines present increased with time. The experimental arrangements were similar to those described above, i.e. the charge trapped on vortex lines was measured by applying the axial electric field thus transferring the charge to a collector attached to an electrometer. The appearance of each new vortex line was detected by a steplike increase in the electrometer's reading. Bringing the container slowly to rest, the authors also discovered the existence of remanent vorticity studied later by Awschalom and Schwarz (see below).

Later Williams and Packard [91] developed the first photographic technique which directly visualized spatial positions of individual quantized vortex lines in rotating ^{4}He. The experimental arrangements were similar to those of Ref. [90], but in addition the magnetic focusing was used to stabilize beams of electrons emitted from the charged vortex lines; these beams impinged on a phosphor screen so that the positions of quantized vortices could be actually photographed. Experiments were performed at temperatures lower than 0.3 K, and up to 0.8% of ^{3}He (which acted as a fixed amount of normal fluid) was added to stabilize the vortices. Among other results, it was found, in agreement with the classical Feynman's prediction, that the average intervortex spacing is $\sim \sqrt{h/2\omega m_4}$, where ω is the angular speed of rotation, but in this work an expected stable triangular lattice of vortices was never observed. The photographs of regular, symmetric arrays of vortices were obtained when this experiment was repeated some years later [92]. (These photographs should be very familiar to a reader through numerous reproductions in other publications and hence are not shown here.) The authors ascribed to mechanical disturbances their earlier failure to observe the regular structures. They also argued that the symmetric state of the system is determined not by the absolute minimum of the free energy, as has been believed earlier, but by the combination of the past history of the system and

the local minimum of the free energy, concluding that the symmetric state is highly metastable. The detailed description of the photographic technique for visualizing the positions of quantized vortices in rotating ^{4}He was given in work [93]. Much later one of the authors claimed [94] that usual helium ions are not really suitable for detection of thermally excited vortices, and that multielectron bubbles should be employed for this purpose. Although such an experiment was outlined in the cited paper, the authors of this review are not aware of any practical development in this direction.

Using the experimental technique of Ref. [91], this research group also revisited [95] the problem, analyzed earlier theoretically by Donnelly, Roberts, and Parks [21, 75–77], of the lifetime of ions trapped on the vortex lines. Theoretical analysis predicted that in the temperature interval $0.6\ \mathrm{K} < T < 1.1\ \mathrm{K}$ the mean lifetime should be longer than 10^{13} s and that it should increase with decreasing temperature. However, the experiments revealed that the observed lifetime was many orders of magnitude smaller and was actually decreasing as temperature decreased. To resolve the contradiction with the theoretical predictions, the authors suggested that at temperatures lower than 1.5 K the trapping lifetime is no longer determined by the intrinsic properties of bubble-vortex interaction but by a time scale of the vortex motion until it is destroyed by the container's wall. The details of this mechanism were suggested by the authors as follows: as the moving vortex filament encounters the wall, it is destroyed (so that the charge is collected by the wall), but, to maintain the equilibrium value of the vortex line density, another, uncharged filament is created. In the case where the time scale of migration of the vortex filament to the wall is smaller than the intrinsic trapping lifetime of the ion bubble, the vortex motion will be a limiting factor of the charge loss. The authors concluded that at low temperatures such that the normal fluid density and hence viscous damping (by the mutual friction) become negligible, the observed lifetime is actually the measure of the timescale of the vortex migration to the wall and, therefore, should be independent of temperature, in agreement with the authors' observations. Furthermore, the authors argued that their conclusions can also be related to the earlier observations by Cheng, Cromar, and Donnelly [96] that the ion trapping reduces in the presence of the axial heat current. The explanation suggested in Ref. [95] is that in the counterflow turbulence the mutual friction enhances the intensity of the vortex motion and hence the rate of destruction of vortices by the wall.

Employing the ion trapping technique, one of the works of key importance for understanding the mechanism of the onset of quantum turbulence is that of Awschalom and Schwarz [97]. This experiment used two parallel plates, immersed in ^{4}He, one of which serves as a charge collector detecting the vortices pinned to both plates. (The experiment aimed, in particular, to support the earlier Schwarz's idea [98, 99], based on his analysis of vortex reconnections, that under some conditions vortex singularities can multiply.) The experiment showed that quiescent ^{4}He contains a rather large number of quantized vortex filaments which are pinned metastably to the parallel plates. The line density of these remanent vortices seems to be history independent, and its existence was established upon going, in temperature, down through the λ transition. (Note that in this work the vortex line density was not measured directly but estimated, considering the rather complicated geometry of electric field lines,

from the measurement of the collected charge.) Awschalom and Schwarz found that the line density of remanent vortices is very close to the critical line density, introduced by Tough [100], below which vortices disappear. The authors' interpretation of the critical line density was that the vortex filaments do not disappear but become immobilized by pinning to the walls and hence cannot be observed by any conventional experimental technique. The authors also justified their ideas by analyzing the evolution of the vortex line density in decaying turbulence produced by ultrasound. They observed that, after the ultrasound has been switched off, L decays not to zero but to the value of the remanent vortex line density. (Earlier experiments of Milliken Schwarz, and Smith [101] produced qualitatively similar results.) The authors concluded that any volume "will be penetrated ab initio by quantized vortices stabilized by surface pinning", and hence all experiments on the evolution of the vortex line density should be interpreted as if L starts from the value corresponding to the remanent vortex line density.

The first attempt of systematic experimental study, by means of the ion trapping technique, of the decay of quantum turbulence was made by Davis, Hendry, and McClintock [102]. In turbulence, generated by the oscillating grid, some ions emitted from the tip get trapped on vortices within the tangle and hence reduce the current arriving at the collector. The evolution of the vortex line density can be estimated from the evolution of this current, and the experiment clearly demonstrated the production and decay of quantum turbulence as well as its spatial distribution. However, this experiment had certain disadvantages. In particular, the value of the vortex line density in the low temperature limit (from 200 down to 22 mK) remained unknown, and the data on trapping cross-sections at these temperature had not yet been available. Nevertheless, this experiment yielded a very useful information on the time scale of decay, and also showed that in the temperature range from 22 to 70 mK the process becomes temperature independent.

Clearly, a modification of the classical ion trapping experimental arrangements was required that would make possible, in the low temperature limit $T < 200$ mK, to measure directly the dynamics of the vortex tangle as well as the trapping cross-sections. Such a new technique was recently developed by Walmsley, Golov and their co-workers [54, 55, 103–105]; the detailed description of the experimental cell and methods can be found in the first two of the cited works.

The experimental cell, mounted on a rotating cryostat, is a cube whose sides are electrodes serving as the charge collectors. In the earlier experiment [54] just one ion emission tip was fitted at the bottom side of the cell, while later experiment [55, 103–106] used two emission tips fitted at the bottom and one of the side plates. In order to provide the means of measuring the spatial properties of the vortex tangle, a difference of electric potential was kept between some of the electrodes to ensure depletion of the ion current emitted by the tips. An analysis of ion trapping by quantized vortices suggests the exponential decay of the ion current, collected by the electrodes, with the vortex line density, so that the latter can be recovered from the measurements of the current $I(t)$ from the relation $L(t)/L_0 = (\sigma d)^{-1} \ln[I(\infty)/I(t)]$, where d is the size of the experimental cell. The turbulence was produced by spin up or/and spin down of the rotating experimental cell.

In Ref. [54] the authors argued in favor of using, as probe particles, the charged vortex rings rather than bare ions. The reason is that the trapping cross-section

of the bare ion bubble is small, $\sigma \sim 10^{-6}$ cm [75–77, 107], and was never measured at temperature below 0.8 K. On the other hand, at low temperatures, in the case where the vortex nucleation velocity, v_c is lower than Landau critical velocity, $v_L \sim 5 \times 10^3$ cm/s, the ion, upon reaching the velocity v_c will nucleate the vortex ring that captures the ion thus forming the stable ion-ring complex. The details of this mechanism can be found in the classical paper by Rayfield and Reif [108] (see also the work by Nancolas, Bowley, and McClintock [109] and Donnely's monographs [72, 73]). While attempting, initially, to repeat the experimental conditions of the work by Davis, Hendry, and McClintock [102], who tried to eliminate nucleation of vortex rings by ions, Walmsley, Golov and their co-authors eventually came to a conclusion that at low temperatures charged rings are preferable as probe particles. The trapping cross-section of the charged ring is of the order of its diameter, $\sigma \sim 1$ μm [110], which is much larger than the trapping cross-section of the bare ion bubble, and hence it is considerably easier to detect quantized vortices by charged rings (as was stated much earlier by Guenin and Hess [111]). Some disadvantage of using charged vortex rings is their dynamics which is more complicated than that of bare ion bubbles (we refer the reader to the theoretical studies [112–114]).

The experimental studies [54, 55] of Walmsley et al. showed that using charged rings rather than bare ions it is possible to detect the change in the vortex line density upon starting and stopping rotation at temperatures from 0.5 down to 30 mK. Monitoring in Ref. [55] the trapping of charged rings by rectilinear vortices generated by slow rotation the authors were able to measure the ring-vortex trapping cross-section at these temperatures. Furthermore, at low temperatures injection of charged rings can be used to create a vortex tangle [103].

An application of this technique to the study of quantum turbulence in the limit $T \to 0$ has already brought some non-trivial results. Thus, Walmsley et al. [104, 105] studied, at temperatures from 1.6 down to 0.08 K, a decay of the homogeneous vortex tangle produced by a sudden spin down of the rotating cell. They found that the decay of the energy flux, ϵ is the same as that of the classical turbulence at high Reynolds numbers, i.e. $\epsilon \sim t^{-3}$, and that the vortex line density decays as $t^{-3/2}$. Most importantly, it was found that at $T \approx 0.8$ K the effective kinematic viscosity, ν_K drops sharply from the value $\nu_K \approx 0.1\kappa$ and approaches $\nu_K \approx 0.003\kappa$ as $T \to 0$. The authors linked this drop to the transition to the new form of turbulence, the so-called "ultraquantum" (or "Vinen" as opposed to the classical, "Kolmogorov") turbulence. This, less structured than (quasi)classical regime of turbulence is characterized by the cascade in which the energy is transferred to smaller scales by Kelvin waves on individual vortex lines (and, therefore, by the absence of any large scale motion). The mechanism of energy dissipation is though to be acoustic: smallest perturbations are emitted as phonons. Clearly, the ultraquantum regime should be characterized by an effective kinematic viscosity, ν_V different from the quasiclassical ν_K.

It should be emphasized, though, that the regime of turbulence in the cited work [104, 105] was essentially quasiclassical due to forcing at large scales (rotation). The existence and properties of ultraquantum regime at temperatures below 0.5 K were addressed a year later in the recent work of Walmsley and Golov [106]. The vortex tangle was produced not by spin down of the rotating cell but by charged vortex rings so that no large-scale flow was generated. It was found that in the ultra-

quantum regime the vortex line density decays as t^{-1}, and that the effective kinematic viscosity of the Vinen turbulence is $\nu_V \approx 0.1\kappa$.

In conclusion of this section we would like to emphasize that the considered so far two experimental techniques of visualization (or, at least, detection) of flow properties in turbulent ^{4}He, i.e. PIV/particle tracking and the ion trapping technique do not compete but rather complement each other. Indeed, the ion trapping technique detects quantized vortices without disturbing the flow, and it is efficient in the low temperature regime; at temperatures above 1.7 K ion bubbles can no longer be trapped on quantized vortices. As strongly emphasized by Charalambous et al. [115], the obvious disadvantage of this technique is that ion bubbles "cannot provide the kind of detailed information about turbulent flow patterns that is available in the case of classical turbulence". We fully endorse this statement. Actual visualization of quantized vortex filaments is also hardly possible (but see some new developments discussed below). On the contrary, solid, micron-size particles being used in the PIV and particle tracking techniques, albeit disturbing the flow, can visualize the normal flow and can even be used to "paint" quantized vortices. However, as was demonstrated in Sects. 2.2.1 and 2.5.3, in the low temperature regime, as $T \to 0$ solid particles do not follow the flow, and, as was shown in Sect. 3.3, most likely cannot be trapped on quantized vortices.

In the remainder of this review we will briefly discuss two new promising techniques that potentially can be used for direct flow visualization.

7.2 Cavitating Electron Bubbles and Metastable He_2 Molecules

The first of these methods is being developed at Brown University by Maris and his colleagues [116–119]. The idea of the method comes from the fact that an application of a negative pressure to ^{4}He leads to an increase of the radius of the ion bubble which explodes, and its size grows substantially when the negative pressure has reached the critical value, P_c. Furthermore, Maris et al. argue that since the pressure around the quantized vortex is reduced due to the Bernoulli effect, the ion bubbles trapped on the vortex have the size larger than those in the bulk of ^{4}He and explode at the critical pressure of smaller magnitude (hence the possibility of direct distinguishing the bubbles trapped on vortices from those in the bulk of helium). In these experiments the pressure variations were produced by an acoustic, ultrasonic transducer generating either focused or planar (as in the last of cited works) sound wave. By choosing a suitable frequency and amplitude of the emitted sound, bubbles can be make so large that they can be visualized by the conventional optical methods (e.g. by a laser beam and a photomultiplier). The other advantage of this method is that it uses neither emission of the electron beam nor the electric field to accelerate the ions. The charged particles are those that already present in the bulk of ^{4}He, either as a result of direct ionization by e.g. cosmic rays, or through the more complicated process involving ionization, production of UV photons, and ejection of electrons from the walls into helium by the photoelectric effect.

The absence of the applied electric field means that electron bubbles, unless they are trapped on quantized vortices, will faithfully follow the normal flow. Indeed, the results of visualization showed that in the weak, laminar counterflow most of the bubbles moved along the streamlines of the normal fluid, but alongside those about 10%

of the observed electron bubbles followed snakelike paths; these could be assumed the electron bubbles trapped by vortices and sliding along vortex filaments.

So far no new information on quantum turbulence has been obtained using this technique, but its relative simplicity has a potential to make it a tool competing with the PIV and particle tracking techniques.

Another, completely new visualization technique is currently being developed by McKinsey and his co-workers [120] at Yale University. This technique employs metastable He_2 triplet molecules, produced e.g. by the radioactive source, which can be excited by two infrared photons from the ground $a^3\Sigma_u^+$ state to the excited $d^3\Sigma_u^+$ state. About 90% of the excited molecules will decay into $b^3\Pi_g$ state emitting photons at 640 nm well separated in the wavelength from the excitation photons and hence can be detected by standard techniques. All excited molecules decay back to the ground state within about 50 ns, so that the process can be repeated many times to make possible a detection of a single molecule.

The authors claim that He_2 molecules should be unaffected by quantized vortices at temperatures above 1 K and so allow the resolution of the normal flow even at the Kolmogorov scale. However, Vinen commented [121] that at sufficiently low temperatures triplet molecules may as well become trapped on quantized vortex core. In this case three-dimensional images of vortex lines can be produced by e.g. stereoscopic imaging.

If successful, the further development of this method may be useful for recovering the velocity field and probability distribution function of the normal velocity fluctuations, and can also provide a new, nonintrusive tool for visualization of quantized vortices.

8 Conclusions

This article reviewed the recent progress in understanding the motion of solid particles and mechanisms of their interactions with both the normal fluid and quantized vortices in turbulent ^{4}He. This problem is addressed in the context of the PIV and the particle tracking techniques recently implemented in ^{4}He, although we were certainly biased (perhaps, not surprisingly, considered our own research expertise) towards theoretical and numerical works and interpretation of experimental results.

The problem of the interaction of particle tracers with the normal fluid and with quantized vortices is difficult, at least in principle: it is three-dimensional, time dependent and strongly nonlinear. This is why the best model available (the two-way coupling model described in Sect. 3) is computationally very expensive. In this review we have shown that, fortunately, some aspects of this particle-vortex interaction can be understood using simpler models, either numerical or analytical, particularly given the insight gained from the two-way coupling model.

Although implemented recently (the first publications date 2002), the PIV and the particle tracking techniques applied to the problem of quantum turbulence in ^{4}He had already produced some new results. Among them: the discovery of large-scale eddies, which do not have an analogue in the classical fluid dynamics, in the thermal counterflow past a cylinder; the wider and flatter, compared to classical, velocity

profile in the turbulent boundary layer; scaling for the time evolution of the parameter characterizing reconnections of quantized vortices; non-Gaussian probability distribution function, with the tail scaled as v^{-3}, of the velocity in decaying quantum turbulence. These results seem to suggest that both the PIV and the particle tracking techniques have great potential for studying quantum turbulence. Besides, the motion of solid particles in turbulent ^{4}He seems to be itself an interesting and non-trivial phenomenon worth the detailed theoretical and experimental study.

Although the review of this rapidly development area of research cannot be comprehensive, we attempted to resolve, where possible, contradictions in theoretical interpretations of recent experimental observations and to address yet unresolved issues.

We also reviewed the related experimental methods, first of all the ion trapping technique which is perhaps the main tool for studying quantized vortices in the low temperature limit. We argue that these two experimental methods, i.e. the PIV/particle tracking and the ion trapping techniques do not compete but complement each other. Indeed, each of these techniques is most efficient in its own temperature and flow regime.

Acknowledgements We are grateful to our collaborators, W.F. Vinen and D. Kivotides who contributed to some of the original research reviewed in this article, and to K.R. Sreenivasan for permission to use, in Sect. 2.4, the results of yet unpublished experimental results of Bewley, Lathrop, Sreenivasan, and Paoletti.

References

1. R.J. Donnelly, A.N. Karpetis, J.J. Niemela, K.R. Sreenivasan, W.F. Vinen, J. Low Temp. Phys. **126**, 327 (2002)
2. D. Celik, S.W. Van Sciver, Exp. Therm. Fluid Sci. **26**, 971 (2002)
3. T. Zhang, S.W. Van Sciver, in *Advances in Cryogenics Engineering*, ed. by S. Breon. AIP Conf. Proc., vol. 613 (AIP, Melville, 2002), p. 1372
4. T. Zhang, D. Celik, S.W. Van Sciver, J. Low Temp. Phys. **134**, 985 (2004)
5. T. Zhang, S.W. Van Sciver, J. Low Temp. Phys. **138**, 865 (2005)
6. T. Zhang, S.W. Van Sciver, Nature Physics **1**, 36 (2005)
7. G.P. Bewley, D.P. Lathrop, K.R. Sreenivasan, Nature **441**, 588 (2006)
8. G.P. Bewley, K.R. Sreenivasan, D.P. Lathrop, Exp. Fluids **44**, 887 (2008)
9. G.P. Bewley, M.S. Paoletti, K.R. Sreenivasan, D.P. Lathrop, Proc. Nat. Acad. Sci. **105**, 13707 (2008)
10. M.S. Paoletti, R.B. Fiorito, K.R. Sreenivasan, D.P. Lathrop, J. Phys. Soc. Jpn. **77**, 111007 (2008)
11. M.S. Paoletti, M.E. Fisher, K.R. Sreenivasan, D.P. Lathrop, Phys. Rev. Lett. **101**, 154501 (2008)
12. M. Raffel, C. Willert, J. Kompenhaus, *Particle Image Velocimetry, a Practical Guide* (Springer, Berlin, 1998)
13. P.-E. Roche, P. Diribarne, T. Didelot, O. Francais, L. Rousseau, H. Willaime, Europhys. Lett. **77**, 66002 (2007)
14. T.R. Auton, J.C.R. Hunt, M. Prud'homme, J. Fluid Mech. **197**, 241 (1988)
15. M.R. Maxey, J.J. Riley, Phys. Fluids **26**, 883 (1983)
16. R. Mei, J. Fluid Mech. **270**, 133 (1994)
17. I. Kim, S. Elghobashi, W.A. Sirignano, J. Fluid Mech. **367**, 221 (1998)
18. D.R. Poole, C.F. Barenghi, Y.A. Sergeev, W.F. Vinen, Phys. Rev. B **71**, 064514 (2005)
19. A. Babiano, J.H.E. Cartwright, O. Piro, A. Provenzale, Phys. Rev. Lett. **84**, 5764 (2000)
20. Y.A. Sergeev, C.F. Barenghi, D. Kivotides, W.F. Vinen, Phys. Rev. B **73**, 052502 (2006)
21. P.E. Parks, R.J. Donnelly, Phys. Rev. Lett. **16**, 45 (1966)
22. Y.A. Sergeev, C.F. Barenghi, D. Kivotides, Phys. Rev. B **74**, 184506 (2006) and Erratum, *Phys. Rev. B* **75**, 019904(E) (2007)
23. N.G. Berloff, P.H. Roberts, Phys. Rev. B **63**, 024510 (2000)

24. O.C. Idowu, A. Willis, C.F. Barenghi, D.C. Samuels, Phys. Rev. B **62**, 3409 (2000)
25. Y.A. Sergeev, S. Wang, E. Meneguz, C.F. Barenghi, J. Low Temp. Phys. **146**, 417 (2007)
26. H.E. Hall, W.F. Vinen, Proc. R. Soc. London, Ser. A **238**, 215 (1956)
27. D. Kivotides, C.F. Barenghi, D.C. Samuels, Science **290**, 777 (2000)
28. G.P. Bewley, D.P. Lathrop, K.R. Sreenivasan, M.S. Paoletti, Private communication (2007)
29. D. Kivotides, C.F. Barenghi, Y.A. Sergeev, Phys. Rev. Lett. **95**, 215302 (2005)
30. O.C. Idowu, D. Kivotides, C.F. Barenghi, D.C. Samuels, J. Low Temp. Phys. **130**, 269 (2000)
31. D. Kivotides, S.L. Wilkin, J. Fluid Mech. **605**, 367 (2008)
32. D. Kivotides, C.F. Barenghi, Y.A. Sergeev, Europhys. Lett. **73**, 733 (2006)
33. D. Kivotides, Y.A. Sergeev, C.F. Barenghi, Phys. Fluids **20**, 055105 (2008)
34. L. Onsager, Nuovo Cim. Suppl. 2 **6**, 249 (1949)
35. K.W. Schwarz, Phys. Rev. B **31**, 5782 (1985)
36. K.W. Schwarz, Phys. Rev. B **38**, 2398 (1988)
37. D.C. Samuels, in *Quantized Vortex Dynamics and Superfluid Turbulence*, ed. by C.F. Barenghi, R.J. Donnelly, W.F. Vinen (Springer, Berlin, 2001), p. 97
38. D. Kivotides, J.C. Vassilicos, D.C. Samuels, C.F. Barenghi, Phys. Rev. Lett. **86**, 3080 (2001)
39. D. Kivotides, C.F. Barenghi, Y.A. Sergeev, J. Low Temp. Phys. **144**, 121 (2006)
40. C.F. Barenghi, D. Kivotides, Y.A. Sergeev, J. Low Temp. Phys. **148**, 293 (2007)
41. D. Kivotides, C.F. Barenghi, Y.A. Sergeev, Phys. Rev. B **75**, 212502 (2007)
42. D. Kivotides, C.F. Barenghi, Y.A. Sergeev, Phys. Rev. B **77**, 014527 (2008)
43. D. Kivotides, C.F. Barenghi, Y.A. Sergeev, Phys. Rev. B **77**, 104512 (2008)
44. K.W. Schwarz, Phys. Rev. A **10**, 2306 (1974)
45. M. Tsubota, S. Maekawa, Phys. Rev. B **47**, 12040 (1993)
46. J. Jäger, B. Schuderer, W. Schoepe, Phys. Rev. Lett. **74**, 566 (1995)
47. R. Hänninen, M. Tsubota, W.F. Vinen, Phys. Rev. B **75**, 064502 (2007)
48. D. Kivotides, Phys. Rev. B **77**, 174508 (2008)
49. D. Kivotides, Phys. Rev. B **78**, 224501 (2008)
50. Y.A. Sergeev, C.F. Barenghi, J. Low Temp. Phys. **156**, 268 (2009)
51. T. Xu, S.W. Van Sciver, Phys. Fluids **19**, 071703 (2007)
52. A. White, N.P. Proukakis, C.F. Barenghi, arXiv:0908.3260 (2009)
53. C.F. Barenghi, Y.A. Sergeev, Phys. Rev. B **80**, 024514 (2009)
54. P.M. Walmsley, A.A. Levchenko, A.I. Golov, J. Low Temp. Phys. **145**, 143 (2006)
55. P.M. Walmsley, A.A. Levchenko, S.E. May, A.I. Golov, J. Low Temp. Phys. **146**, 511 (2007)
56. G. Careri, F. Scaramuzzi, J.O. Thomson, Nuovo Cimento **13**, 186 (1959)
57. G. Careri, F. Scaramuzzi, J.O. Thomson, Nuovo Cimento **18**, 957 (1960)
58. G. Careri, in *Progress in Low Temperature Physics, vol. 3*, ed. by C.J. Gorter (Interscience, New York, 1961), p. 58
59. G. Careri, W.D. McCormick, F. Scaramuzzi, Phys. Lett. **1**, 61 (1962)
60. F. Reif, L. Meyer, Phys. Rev. **119**, 1164 (1960)
61. L. Meyer, F. Reif, Phys. Rev. Lett. **5**, 1 (1960)
62. L. Meyer, F. Reif, Phys. Rev. **123**, 727 (1961)
63. R.A. Ferrel, Phys. Rev. **108**, 167 (1957)
64. C.G. Kuper, Phys. Rev. **122**, 1007 (1961)
65. J. Jortner, N.R. Kestner, S.A. Rice, M.H. Cohen, J. Chem. Phys. **43**, 2614 (1965)
66. K. Hiroike, N.R. Kestner, S.A. Rice, J. Jortner, J. Chem. Phys. **43**, 2625 (1965)
67. J. Levine, T.M. Sanders, Phys. Rev. Lett. **8**, 159 (1962)
68. C.G. Kuper, in *Liquid Helium*, ed. by G. Careri. Proc. Enrico Fermi Int. School of Physics (Academic Press, New York, 1963). Course XXI
69. A.J. Dahm, T.M. Sanders, Phys. Rev. Lett. **17**, 126 (1966)
70. A.J. Dahm, T.M. Sanders, J. Low Temp. Phys. **2**, 199 (1970)
71. R.M. Ostermeier, K.W. Schwarz, Phys. Rev. A **5**, 2510 (1972)
72. R.J. Donnelly, *Experimental Superfluidity* (University of Chicago Press, Chicago, 1967)
73. R.J. Donnelly, *Quantized Vortices in Helim II* (Cambridge University Press, Cambridge, 1991)
74. K.R. Atkins, Phys. Rev. **116**, 1339 (1959)
75. R.J. Donnelly, Phys. Rev. Lett. **14**, 39 (1965)
76. R.J. Donnelly, P.H. Roberts, in *Superfluid Helium*, ed. by J.F. Allen (Academic Press, New York, 1966)
77. R.J. Donnelly, P.H. Roberts, Proc. R. Soc. (London) A **312**, 519 (1969)

78. B.E. Springett, Phys. Rev. **155**, 139 (1967)
79. B.E. Springett, D.J. Tanner, R.J. Donnelly, Phys. Rev. Lett. **15**, 585 (1965)
80. D.J. Tanner, Phys. Rev. **152**, 121 (1966)
81. R.L. Douglass, Phys. Rev. Lett. **13**, 791 (1964)
82. A.G. Cade, Phys. Rev. Lett. **15**, 238 (1965)
83. B.E. Springett, R.J. Donnelly, Phys. Rev. Lett. **17**, 364 (1966)
84. W.P. Pratt, W. Zimmermann, Phys. Rev. **177**, 412 (1969)
85. W.I. Glaberson, J. Low Temp. Phys. **1**, 289 (1969)
86. J.A. Northby, R.J. Donnelly, Phys. Rev. Lett. **25**, 214 (1970)
87. M. Vicenti-Missoni, S. Gunsolo, Phys. Rev. **144**, 196 (1966)
88. D.M. Sitton, F. Moss, Phys. Rev. Lett. **23**, 1090 (1969)
89. W.F. Vinen, Proc. R. Soc. (London) A **242**, 493 (1957)
90. R.E. Packard, T.M. Sanders, Phys. Rev. A **6**, 799 (1972)
91. G.A. Williams, R.E. Packard, Phys. Rev. Lett. **33**, 280 (1974)
92. E.J. Yarmchuk, M.J.V. Gordon, R.E. Packard, Phys. Rev. Lett. **43**, 214 (1979)
93. G.A. Williams, R.E. Packard, J. Low Temp. Phys. **39**, 553 (1980)
94. G.A. Williams, Z. Phys. B **98**, 341 (1995)
95. K. DeConde, G.A. Williams, R.E. Packard, Phys. Rev. Lett. **33**, 683 (1974)
96. D.K. Cheng, M.W. Cromar, R.J. Donnelly, Phys. Rev. Lett. **31**, 433 (1973)
97. D.D. Awschalom, K.W. Schwarz, Phys. Rev. Lett. **52**, 49 (1984)
98. K.W. Schwarz, Phys. Rev. Lett. **49**, 283 (1982)
99. K.W. Schwarz, Phys. Rev. Lett. **50**, 364 (1983)
100. J.T. Tough, in *Progress in Low Temperature Physics*, ed. by D.F. Brewer (North-Holland, Amsterdam, 1982), p. 133
101. F.P. Milliken, K.W. Schwarz, C.W. Smith, Phys. Rev. Lett. **48**, 1204 (1982)
102. S.I. Davis, C. Hendry, P.V.E. McClintock. Physica B **280**, 43 (2000)
103. P.M. Walmsley, A.I. Golov, A.A. Levchenko, B. White, J. Low Temp. Phys. **148**, 317 (2007)
104. P.M. Walmsley, A.I. Golov, H.E. Hall, A.A. Levchenko, W.F. Vinen, Phys. Rev. Lett. **99**, 265302 (2007)
105. P.M. Walmsley, A.I. Golov, H.E. Hall, W.F. Vinen, A.A. Levchenko, J. Low Temp. Phys. **153**, 127 (2008)
106. P.M. Walmsley, A.I. Golov, Phys. Rev. Lett. **100**, 245301 (2008)
107. R.M. Ostermeier, W.I. Glaberson, J. Low Temp. Phys. **25**, 317 (1976)
108. G.W. Rayfield, F. Reif, Phys. Rev. A **136**, 1194 (1964)
109. G.G. Nancolas, R.M. Bowley, P.V.E. McClintock, Philos. Trans. R. Soc. (Lond.) A **313**, 537 (1985)
110. K.W. Schwarz, R.J. Donnelly, Phys. Rev. Lett. **17**, 1088 (1966)
111. B.M. Guenin, G.B. Hess, J. Low Temp. Phys. **33**, 243 (1978)
112. C.F. Barenghi, R.J. Donnelly, W.F. Vinen, J. Low Temp. Phys. **52**, 189 (1983)
113. D.C. Samuels, R.J. Donnelly, Phys. Rev. Lett. **67**, 2505 (1991)
114. M. Tsubota, H. Adachi, *J. Low Temp. Phys.* (2009, in print)
115. D. Charlambous, P.C. Hendry, M. Holmes, G.G. Ihas, P.V.E. McClintock, L. Skrbek, J. Low Temp. Phys. **145**, 107 (2006)
116. J. Classen, C.-K. Su, M. Mohazzab, H.J. Maris, Phys. Rev. B **57**, 3000 (1998)
117. J. Classen, C.-K. Su, M. Mohazzab, H.J. Maris, J. Low Temp. Phys. **110**, 431 (1998)
118. A. Ghosh, H.J. Maris, Phys. Rev. Lett. **95**, 265301 (2005)
119. W. Guo, H.J. Maris, J. Low Temp. Phys. **148**, 199 (2007)
120. W.G. Rellerget, S.B. Cahn, A. Garvan, J.C. Hanson, W.H. Lippincott, J.A. Nikkel, D.N. McKinsey, Phys. Rev. Lett. **100**, 025301 (2008)
121. W.F. Vinen, in *Low Temperature Physics*. AIP Conf. Proc., vol. 850 (AIP, New York, 2006), p. 169